Seasonal modes of dryness and wetness variability over Europe and their connections with large scale atmospheric circulation and global sea surface temperature

M. Ionita (1)

(1) Alfred Wegener Institute Helmholtz Centre for Polar and Marine Research, Bremerhaven, Germany

C. Boroneanț (2)

(2) Center for Climate Change, Geography Department, University Rovira I Virgili, Tortosa, Spain

S. Chelcea (3)

National Institute of Hydrology and Water Management, Bucharest, Romania

Corresponding author:

Email: Monica.Ionita@awi.de

Address: Alfred Wegener Institute Helmholtz Centre for Polar and Marine Research
Bussestrasse 24
D-27570 Bremerhaven

Germany
Telephone: +49(471)4831-1845

Fax: +49(471)4831-1271

Abstract

The relationship between the seasonal modes of interannual variability of a multiscalar drought index over Europe and the large-scale atmospheric circulation and sea surface temperature (SST) anomaly fields is investigated through statistical analysis of observed and reanalysis data. It is shown that the seasonal modes of dryness and wetness variability over Europe and their relationship with the large-scale atmospheric circulation and global sea surface temperature anomaly fields differ from one season to another. During winter, the dominant modes of dryness and wetness variability are influenced by the Arctic Oscillation (AO)/North Atlantic Oscillation (NAO), the Scandinavian pattern (SCA), the East Atlantic pattern (EA) and the East Atlantic/Western Russia (EAWR) pattern. The spring dryness/wetness modes are influenced mainly by the Arctic Oscillation (AO), Polar/Eurasian patterns (POL) and the Atlantic Multidecadal Oscillation (AMO) conditions. The phases (positive or negative) and the superposition of these large scale variability modes play a significant role in modulating the drought conditions over Europe. During summer, the atmospheric blocking is one of the main drivers of dryness and wetness conditions, while during autumn dryness/wetness conditions variability can be related to the NAO or with a wave train like pattern in the geopotential height at 850mb, which develops over the Atlantic Ocean and extends up to Siberia. It is also found that the response of the dryness and wetness conditions to global SST is more regional in summer, compared to the other seasons, when local processes may play a more important role.

1. Introduction

Drought is more than a physical phenomenon or a natural event. Its impact results from the relation between a natural event and demands on the water supply, and it is often exacerbated by human activities. In the context of climate change, the frequency and intensity of drought are changing and their social and economic impact increase. Moreover, drought is one of the most complex phenomena which may have a strong impact on agriculture, society, water resources and ecosystems. One of the reasons for this is the spatial extent of drought and its duration, sometimes reaching continental scales and lasting for many years. Usually, drought is defined as a period of deficient precipitation over a long period of time (e.g a season or more). Typically, there are four types of drought: a) *meteorological drought* (characterized by months to years with precipitation deficit), b) *agricultural drought* (this includes the soil drought and soil-atmospheric drought, and is characterized by dry soils as a direct effect of reduced precipitation) c) *hydrological drought* (occurs when river streamflow and the water storages fall bellow long-term mean levels) and d) *socio-economic drought* (occurs when the demand for an economic good exceeds supply as a result of a weather-related shortfall in water supply) (Ped, 1957; WMO, 1975; Wilthie and Glantz, 1985; Farago et al., 1989; Maracchi, 2000; Dai, 2011a).

Dryness and wetness fluctuations can have an overwhelming effect on hydrology, agriculture, water management and ecosystems (Tao et al., 2014). To monitor and quantify dryness and wetness, various indices have been developed. However, a unique and universally accepted indicator does not exist yet (Heim, 2002; Dai, 2011b). One of the most used indices is the Palmer Drought Severity Index (PDSI) (Palmer, 1965). The PDSI is based on a supply-and-demand model of soil moisture and it enables the measurement of both wetness (positive values) and dryness (negative values). The index has proven to be the most effective in determining long-term dryness and wetness — a matter of several months — and not as good with conditions over a matter of weeks (Alley, 1984; Weber and Nkemdirim, 1998). One of the main disadvantages of PDSI is that it has a fixed temporal scale and does not allow the identification of different types of drought (e.g. agricultural, hydrological or meteorological). This may act as a drawback because drought is considered a multiscalar phenomenon (McKee et al., 1993, Vicente-Serrano et al, 2010). An improvement was made by McKee et al. (1993) with the development of the Standardized Precipitation Index (SPI), which takes into account the multiscalar nature of droughts. But SPI has a major drawback: it is based only on precipitation and does not take into account the effect of evapotranspiration, which has a strong

impact on drought conditions. Recently, a new indicator the Standardized Precipitation - Evapotranspiration Index (SPEI) (Vicente – Serrano, 2010) has been developed to quantify the drought condition over a given area. SPEI takes into account both precipitation and evapotranspiration and can be computed on time scales from 1 to 48 months. SPEI combines the sensitivity of PDSI to changes in evaporation demand with the multiscalar nature of SPI. More detailed description of SPEI and the method of computation are given by Vicente-Serrano et al. (2010).

During the last 150 years there has been a global temperature increase (0.5°C - 2°C) (Jones and Moberg, 2003) and climate models project a marked increase in global temperature during the twenty-first century (Solomon et al., 2007). An increase in global temperatures is very likely reflected in precipitation and atmospheric moisture, via induced changes in atmospheric circulation, a more intense hydrological cycle and an increase in the water holding capacity throughout the atmosphere (Folland et al., 2001). As a consequence it is very important to define a drought index which can take into account both the effect of precipitation and temperature (throughout the potential evapotranspiration). Recent studies have shown the importance of temperature in explaining recent trends in water resources (Nicholls, 2004; Cai and Cowan, 2008, Vicente-Serrano et al., 2010). Dai (2011a) and Vicente-Serrano et al. (2010) suggested that the increasing drying trends detected in the PDSI and SPEI global datasets, over many land areas, are due to a certain degree to the increasing temperature trend since the mid-1980s.

At the European scale, research on drought and wetness variability has been mainly focused on regional scales and/or over regions which became more exposed to severe droughts: Iberian Peninsula (Estrela et al., 2000; Vicente-Serrano, 2011), the Mediterranean region (Livada and Assimakopolous, 2007), south-eastern Europe (Koleva and Alexandrov, 2008) and central Europe (Potop et al. 2013; Boroneant et al., 2012). Looking at other European regions, Briffa et al. (2009) showed that high summer temperatures in the western and central part of Europe are responsible for the large extent of summer drought conditions. Trnka et al (2009) emphasized that the drought conditions in the central part of Europe are triggered by different atmospheric circulation patterns and that the drought phenomenon is very pronounced in early vegetation period (April – June). Ionita et al. (2012a) showed that summer drought conditions over Europe can also be influenced by the previous winter SST anomalies in key regions and by a combination of different oceanic and atmospheric modes of variability like Atlantic Multidecadal Oscillation (AMO), Pacific Decadal Oscillation (PDO) and North Atlantic Oscillation (NAO). Altogether, when favorable phase

conditions are met, both these large scale atmospheric and oceanic factors could act as precursors for summer drying conditions over Europe. Although the aforementioned studies already investigated the dryness and wetness variability over Europe, they are either regional in terms of spatial extent or restricted to a particular season. Except the study of Lloyd-Hughes and Saunders (2002), which provides an analysis of drought climatology for Europe in terms of strength, number of events, mean and maximum duration of droughts, to the authors´ knowledge there is no other recent study that deals with a comprehensive analysis of the short term seasonal dryness/wetness conditions over Europe and with the link between the dryness and wetness variability and the large-scale atmospheric circulation and global SST.

Motivated by the above mentioned considerations, this paper focuses on a comprehensive analysis of the seasonal dryness and wetness variability over Europe. Taking this into account, the main goals of this study are: i) to quantitatively describe the seasonal leading modes of dryness/wetness variability over Europe and ii) to determine to what extent the seasonal dryness and wetness variability over Europe are influence by the large-scale atmospheric circulation and global sea surface temperature. The composites of geopotential height at 850hPa (Z850) and global sea surface temperature (SST) anomalies and the correlation maps of number of rain days (WET), cloud cover (CLD) and soil moisture (SOIL) with the principal components corresponding to the main modes of SPEI variability are used to explain the seasonal dryness and wetness variability. These large scale patterns can provide information on the mechanisms by which the large scale factors can influence the European dryness and wetness variability.

This paper is organized as follows: the data sets used in this study and the methods employed are described in section 2. The spatio-temporal variability of the seasonal dryness/wetness, quantified by the SPEI over Europe, is presented in section 3. The relationships between the leading modes of SPEI variability and the Northern Hemisphere atmospheric circulation and global sea surface temperature are examined in section 4 and the link between the seasonal SPEI variability and three climate parameters like the number of rain days, cloud cover and soil moisture is analyzed in section 5. In section 6 a discussion on the results is presented, while the main conclusions are outlined in section 7.

2. Data and methods

2.1 Data

To calculate the Standardized Precipitation-Evapotranspiration Index (SPEI) we used monthly

precipitation totals, 2m surface air temperature means and potential evapotranspiration data from the CRU T.S. 3.20 dataset (Harris et al., 2013), with a spatial resolution of 0.5° X 0.5°. From the same data set we also used two meteorological parameters: monthly number of rain days (WET) and cloud cover fraction (CLD). Since the focus of this study is the short-time dryness and wetness variability, SPEI for 3 months accumulation period (SPEI3 from now on) was calculated.

To investigate the relationship of SPEI3 with global sea surface temperature we used the Hadley Centre Sea Ice and Sea Surface Temperature data set – HadISST (Rayner et al., 2003). This data set covers the period 1871 – 2012 and has a spatial resolution of 1° x 1°. For the present study we only used the data for the period 1901 – 2012.

To investigate the link between the seasonal modes of SPEI3 variability and the Northern Hemisphere atmospheric circulation we used the seasonal means of Geopotential Height at 850mb (Z850), the zonal wind (u850) and the meridional wind (V850) at 850mb from the Twentieth Century Reanalysis (V2) data set (NCEPv2, Whitaker et al., 2004; Compo et al., 2006; Compo et al., 2011) on a 2ºx2º grid, for the period 1901-2012. The Soil Moisture dataset is extracted from the same data set. In this study, we use the soil moisture content in the top layer.

We also used the time series of monthly teleconnection indices described in Table 2. From the monthly time series the seasonal means were computed by averaging the months December/January/February (DJF), March/April/May (MAM), June/July/August (JJA) and September/October/November (SON), respectively. The time series of the Northern Hemisphere teleconnection indices were detrended and normalized by their corresponding standard deviation.

2.2 Methods

The primary quantity analyzed in this study is the Standardized Precipitation-Evapotranspiration Index (SPEI). SPEI is similar to the Standardized Precipitation Index (SPI) (McKee et al., 1993) but it includes the role of temperature. SPEI is a multi-scalar drought indicator based on monthly precipitation totals (PP) and temperature means. The algorithm to calculate the SPEI uses the monthly difference between total precipitation (PP) and Potential Evapotranspiration (PET) which represents a simple climatic water balance calculated at different time-lags to obtain the SPEI for different accumulation period (Vicente-Serano et al., 2010). The estimation of PET is based on the Penmann-Monteith method (Vicente-Serano et al., 2010).

The patterns of the dominant modes of SPEI3 variability are based on Empirical Orthogonal Function (EOF) analysis (e.g. von Storch and Zwiers, 1999). The EOF technique aims at finding a

new set of variables that captures most of the observed variance from the data through a linear combination of the original variables. The EOF analysis represents an efficient method to investigate the spatial and temporal variability of time series which cover large areas. This method splits the temporal variance of the data into orthogonal spatial patterns called empirical eigenvectors. In this study the EOF was applied to the detrended anomalies of the seasonal SPEI3. For all seasons we retained just the first three leading modes, which together account for more than 40% of the total explained variance. These EOF's are well separated according to the North rule (North et al., 1982, *Table 1*). To better identify the periods characterized by persistent dryness/wetness the principal component (PCs) time series were smoothed with a centered 7-year running mean.

Due to data availability constraint the correlation coefficients between the time series of principal components (PCs) corresponding to the first three seasonal EOFs of SPEI3 and the Northern Hemisphere teleconnection indices were calculated over the common period 1950 – 2012 ((*Table 3*). To identify the physical mechanisms responsible for the connection between SPEI3 seasonal variability and large-scale atmospheric circulation and global SST, we constructed the composite maps of Z850 and global SST standardized anomalies for each season by selecting the years when the value of normalized time series of coefficients of the first three standardized SPEI3 PCs was > 1 std. dev (High) and < -1 std. dev (Low), respectively. This threshold was chosen as a compromise between the strength of the climate anomalies associated to SPEI3 anomalies and the number of maps which satisfy this criterion. Further analysis has shown that the results are not sensitive to the exact threshold value used for the composite analysis (not shown). The selected years according to this criteria that were used to build up the composite maps are shown in *Table 4*, for each time series of the seasonal PCs. To better emphasize the difference between wet and dry conditions the maps corresponding to the difference between High – Low years are shown and discussed.

3. Leading modes of dryness and wetness variability and their relationship with the Northern Hemisphere teleconnection patterns

3.1 Winter

The first leading mode for winter SPEI3 (Figure 1a), which describes 21.2% of the total variance, is characterized by positive loadings over the whole Europe with few exceptions located over the north-western part of the Scandinavian Peninsula and the southern half of the Iberian Peninsula. The corresponding PC1 time series of coefficients presents pronounced interannual variability (Figure 1d) and is negatively correlated with the time series of the winter EAWR index (r= - 0.24, 90%

significance level, *Table 3*). The driest winters, in terms of winter PC1 (Figure 1d), were recorded for the years 1909, 1921, 1949 and 1954, while the wettest years were recorded in 1948, 1966, 1967 and 1981, respectively.

The second winter EOF of SPEI3 (Figure 1b), explaining 13.6% of the total variance, shows a dipole-like structure, with negative loadings over the central and southern part of Europe and positive loadings over the Scandinavian Peninsula. The corresponding principal component (PC2) time series of coefficients presents s strong interannual variability component, which can be inferred from the time evolution of the winter PC2 time series of coefficients (Figure 1e). Moreover, from the beginning of 1980's until 2012, the winter PC2 time series of coefficients is characterized by a persistent period of positive anomalies, implying that the Scandinavian Peninsula has been exposed to prolonged wetness, while the southern part of Europe has been exposed, over the last 30 years, to a period of prolonged winter dryness. The winter PC2 time series of coefficients is negatively correlated with the winter time series of the Scandinavian (SCA) teleconnection pattern (r = -0.56, 99% significance level, *Table 3*) (Barnston and Livezey, 1987) and with the winter Niño4 index (r= - 0.22, 90% significance level, *Table 3*). Also, the winter PC2 time series of coefficients is positively correlated with the winter time series of the North Atlantic Oscillation (NAO)/Arctic Oscillation (AO) patterns (r = 0.64/ r=0.79, 99% significance level, *Table 3*) and with the winter time series of the East Atlantic/Western Russia (EAWR) pattern (r = 0.34, 99% significance level, *Table3*). Notably, the DJF PC2 time series of coefficients shows an upward trend after 1950s (Figure 1e). The driest years, for winter PC2 (Figure 1e), were recorded for three consecutive winters: 1940 – 1942 and for the winter 1947, while the wettest years, in terms of winter PC2, were recorded for the years 1949, 2008 and 2012, respectively.

The third winter EOF of SPEI3 (8.8% explained variance) has a tripole-like structure (Figure 1c) with positive loadings over the north-western part of the Scandinavian Peninsula, negative loadings over the southern part of the Scandinavian Peninsula, central and western part of Europe, and positive loadings over the Balkans, eastern Europe and the central part of Russia. Outside these regions the EOF3 loadings are close to zero. The winter PC3 time series of coefficients is negatively correlated with the winter time series of the EA and SCA patterns (r = -0.28, 95% significance level, and r = -0.39, 99% significance level, respectively, *Table 3*) and positively correlated with the winter time series the EAWR pattern (r = 0.28, 95% significance level, *Table 3*). As in the case of winter PC2, the variability of drought conditions related to PC3 is the result of the overlap of several climate modes. The driest years, in term of winter PC3 (Figure 1f), were recorded in 1930, 1936,

1945 and 2001, while the wettest years were recorded for the winters 1905, 1963, 1984 and 2002, respectively.

3.2 Spring

The first spring EOF pattern of SPEI3 (Figure 2a), which explains 21.2% of the total variance, is characterized by positive loadings over the Scandinavian Peninsula and most part of Europe and negative loadings over the Iberian Peninsula and the southernmost part of Europe. The corresponding time series of coefficients (PC1 MAM) is characterized by a pronounced interannual variability (Figure 2d). Spring PC1 time series of coefficients is positively correlated with the spring time series of the EA pattern (r = 0.35, 99% significance level, Table3) and negatively correlated with the spring time series of the Polar/Eurasian pattern (POL) (r = -0.26, 95% significance level, *Table 3*) and the spring time series of the SCA pattern (r = -0.42, 99% significance level, *Table3*). The driest years, in terms of spring PC1 (Figure 2d), were recorded in 1918, 1974 and 1996, while the wettest years were recorded in 1966, 1992, 2000 and 2008, respectively.

The second spring EOF pattern of SPEI3 which explains 14.0% of the total variance features a dipole like pattern between the Scandinavian Peninsula and the rest of Europe (Figure 2b). The highest positive loadings are centered over Norway, while the highest negative values are centered over central Europe and the Balkans. PC2 MAM time series of coefficients (Figure 2e) emphasizes both inter-annual and decadal (~20 years) variability. Spring PC2 time series is positively correlated with the time series of spring Arctic Oscillation (AO) index (r = 0.52, 99% significance level, *Table 3*) and negatively correlated with the spring time series of SCA index (r = -0.49, 99% significance level, *Table 3*). The driest years, according to spring PC2 (Figure 2e), were recorded in 1919, 1923, 1941 and 1969, while de wettest years were recorded in 1921, 1938 and 1997, respectively.

The third spring EOF pattern of SPEI3 (Figure 2c), explaining 8.6% of the total variance, emphasizes a dipole-like structure between the eastern part of Europe and Russia (positive loadings) and the western part of Europe (negative loadings). Spring PC3 time series of coefficients presents both interannual as well as decadal variability (Figures 3f). Spring PC3 time series of coefficients is significantly positively correlated with the spring time series of the Atlantic Multidecadal Oscillation (AMO) index (r = 0.37, 99% significance level, *Table 3*). The AMO warm phase since the early 1930s up to 1960s is associated with positive values of PC3 coefficients, while the cold phase of AMO from the beginning of 1970s up to 1990s is associated with predominantly negative values of spring PC3 coefficients (Figure 2f). The driest years, in terms of spring PC3 time series of

coefficients, were recorded in 1928, 1934, 1937 and 1972, while de wettest years were recorded in 1929, 1938, 1944 and 1953, respectively.

3.3 Summer

The pattern of summer EOF1 of SPEI3 (12.0% of the total variance) (Figure 3a) emphasizes a north-south dipole between the Scandinavian Peninsula and the northern part of Europe (positive loadings) and the southern part of Europe (negative loadings). The corresponding PC1 time series shows pronounced decadal to multidecadal variability (Figure 3d). The time series of summer PC1 of coefficients is negatively correlated with the summer time series of the EAWR pattern (r = -0.47, 99% significance level, *Table 3*), the summer NAO/AO pattern (r = -0.55/ r = -0.31, 99% significance level, *Table 3*), the summer SCA pattern (r = -0.46, 99% significance level, *Table 3*) and positively correlated with the time series of summer AMO pattern (r = 0.27, 95% significance level, *Table 3*) and the summer EA pattern (r = 0.40, 99% significance level, *Table 3*). The driest summers, in terms of summer PC1 (Figure 3d), were recorded for the years 1927, 1928, 1985, 1992 and 2012, while the wettest summers, in terms of summer PC1, were recorded for the years 1914, 1940, 1941, 1959 and 1992, respectively.

The pattern of the second EOF of summer SPEI3 (Figure 3b), which explains 9.4% of the total variance, shows strong negative loadings over the western Russia and strong positive loadings over the Scandinavian Peninsula and Turkey. The time series of coefficients of summer SPEI3 PC2 shows both interannual and decadal variability (Figures 4e). The time series of coefficients of summer PC2 is negatively correlated with the time series of summer EAWR index (r = -0.27, 95% significance level, *Table 3*). The driest summer years, in terms of summer PC2 (Figure 3e), were recorded for the years 1933, 1941, 1978 and 1980, while the wettest summers, in terms of summer PC2, were recorded for the years 1936, 1981 and 1992, respectively.

The pattern of summer EOF3 of SPEI3 (Figure 3c), explaining 8.3% of the total variance, is characterized by negative loadings over the western Russia and north-western Scandinavia, and positive loadings over the eastern, central and most of the western part of Europe. The time series of coefficients of summer PC3 is negatively correlated with the time series of summer AO/NAO indexes (r = -0.31 / r = -0.26, 99%/95% significance level, *Table 3*) and positively correlated with the time series of summer EA index (r = 0.25, 95% significance level, *Table 3)* and the time series of summer SCA index (r = 0.21, 90% significance level, *Table 3*) (Figure 3d). The driest years, according to summer PC3 (Figure 3f), were recorded in 1904, 1921 and 1976, while the wettest

311 years were recorded in 1910, 1972, 1980 and 1997, respectively.
312
313 **3.4 Autumn**

314 During autumn, the leading EOF mode of SPEI3 (Figure 4a) accounts for 15.0% of the total
315 variance. The spatial pattern of this mode is characterized by negative loadings over the
316 southernmost part of Europe and Turkey, and positive loadings over the central and northern part of
317 Europe, the Scandinavian Peninsula and western Russia. The time series of coefficients of autumn
318 PC1 of SPEI3 (Figures 4d) shows enhanced multidecadal variability since 1901 until the beginning
319 of 1980s. After this period the PC1 time series mainly presents interannual variability. The time
320 series of PC1 coefficients for autumn SPEI3 is negatively correlated with the time series of indices
321 associated with the autumn POL teleconnection pattern (r = -0.34, 99% significance level, *Table 3*)
322 and with the autumn time series of the EAWR pattern (r = -0.25, 95% significance level, *Table 3*).
323 The driest autumns, in terms of autumn PC1 (Figure 4d), were recorded for the years 1920, 1951
324 and 1959, while the wettest years were recorded in 1923,1930, 1952 and 1954, respectively.
325 The second EOF mode of autumn SPEI3 variability (Figure 4b) explains 12.2% of the total variance.
326 Structurally, this pattern resembles the second EOF mode of winter and spring, being characterized
327 by negative loadings over the central and eastern part of Europe and positive loadings over the
328 Scandinavian Peninsula. The time series of PC2 coefficients is positively correlated with the time
329 series of autumn AO/NAO indices (r = 0.52/ r = 0.37, 99% significance level, *Table 3*) and
330 negatively correlated with the time series of autumn SCA index (r = -0.33, 99% significance level,
331 Table3). The driest years, based on autumn PC2 (Figure 4e), were recorded in 1922, 1939 and 1960,
332 while the wettest years, in terms of autumn PC2, were recorded for the years 1942, 1961, 1983 and
333 2011, respectively.
334 The third EOF mode of SPEI3 for autumn (Figure 4c), explaining 8.8% of the total variance, is
335 characterized by positive loadings over the western part of Russia and the coastal region of the
336 Scandinavian Peninsula and negative loadings over the western, central and south-eastern part of
337 Europe. Outside these regions the loadings are close to zero. The time series of PC3 coefficients
338 shows strong interannual variability (Figure 4d). The time series of coefficients for autumn PC3 of
339 SPEI3 is positively correlated with the time series of autumn AO/NAO indices (r = 0.31/ r = 0.31,
340 99% significance level, *Table 3*) and the time series of autumn EAWR index (r = 0.26, 95%
341 significance level, *Table 3*) and negatively correlated with the time series of autumn SCA index (r =
342 -0.39, 99% significance level, Table3). The driest years, in term of autumn PC3 (Figure 4f), were

343 recorded in 1924, 1938, 1944 and 1974, while the wettest years were recorded for the autumns 1947,
344 1978 and 2003, respectively.
345

346 # 4. Relationship with large-scale atmospheric circulation and global SST

347 To identify the physical mechanisms responsible for the connection between SPEI3 seasonal
348 variability and large-scale atmospheric circulation and global SST, we constructed the composite
349 maps of the standardized anomalies of Z850, wind vectors at 850mb (W850) and global SST for
350 each season by selecting the years when the value of normalized time series of coefficients of the
351 first three PCs were > 1 std. dev (High) and < -1 std. dev (Low), respectively. In Figures 5 - 8 we
352 will show and discus just the difference between the High – Low maps.

353 ## 4.1 Winter

354 Figure 5 shows the composite maps of winter anomalies (High-Low) of Z850 and W850 (left panels)
355 and global SST (High-Low) (right panels) corresponding to the above mentioned selection criteria.
356 Positive values of the standardized winter PC1 of SPEI3 are associated with a center of negative
357 Z850 anomalies over the whole Europe and central North Atlantic and, a center of positive Z850
358 anomalies over Canada, Greenland up to Siberia (Figure 5a). This pattern is associated with
359 enhanced precipitation over the central part of Europe and reduced precipitation over the northern
360 part of the Scandinavian Peninsula. High values of winter standardized PC1 coefficients are also
361 associated with a tripole-like SST pattern, characterized by a cold center of SST anomalies over the
362 Gulf of Mexico and the eastern US coast, positive SST anomalies in the central North Atlantic that
363 extends from the southern Greenland towards the tropical Atlantic Ocean and a center of negative
364 SST anomalies over the North Sea and the surrounding areas (Figure 5d). Such kinds of Z850 and
365 SST anomalies induce wet conditions over most of the European regions, in agreement with the
366 winter EOF1 pattern (Figure 1a), via the advection of warm and moist air (see the wind vectors in
367 Figure 5a) from the tropical and the eastern coast of the North Atlantic Ocean (positive SST
368 anomalies in Figure 5d).
369 The composite map of winter anomalies of Z850 and W850 (Figure 5b) based on the selected PC2
370 values fulfilling the criteria is characterized by a region of negative anomalies over Greenland, the
371 Scandinavian Peninsula and Siberia and an extended region of positive anomalies which covers the
372 central North Atlantic Ocean and the whole Europe and the Mediterranean region. This pattern
373 resembles the positive phase of the AO/NAO. In section 3.1 we have identified that winter PC2 time

series of coefficients of SPEI3 is significantly correlated with both, the winter AO/NAO index as well as with the winter SCA index. From this finding we can argue that the second winter mode of SPEI3 variability is influenced by a combination of the different climatic modes and teleconnections. This is not so surprising, especially in the context of recent findings of Comas-Bru and McDermott (2013) showing that NAO centers of action are influenced by the phases of the East Atlantic (EA) and SCA patterns, whereas precipitation and temperature over U.K. and the northern part of Europe are differently correlated to NAO, depending on the SCA phase. Positive values of winter PC2 of SPEI3 are also associated with negative SST anomalies in the central tropical Pacific flanked by positive SST anomalies in the central north Pacific and central south Pacific (Figure 5e). This pattern resembles the SST pattern associated to the cold phase of El Niño – Southern Oscillation (ENSO) and it is consistent with the results of previous studies which showed that ENSO has a strong influence on the river streamflow in Europe (Rimbu et al., 2004; Ionita et al., 2008; 2009; 2012b), on precipitation over Europe (Marriotti et al., 2002; van Oldenburgh et al., 2000) and on diurnal temperature range over Europe (Ionita et al., 2012c). It is also consistent with the results presented in Section 3 showing that the time series of standardized coefficients of winter PC2 of SPEI3 is significantly correlated with the winter Niño 4 index ($r = -0.22$, 90% significance level, see Table 3). It is worth to note that the positive values of winter PC2 of SPEI3 are also associated with a tripole-like SST pattern over the North Atlantic region, but it is different in its spatial structure to the one associated to winter PC1. It is characterized by positive SST anomalies along the eastern US coast, European coast and the North Sea and negative SST anomalies in the tropical Atlantic Ocean and south of Greenland. Such a SST pattern resembles the SST anomalies associated with the positive phase of the AO/NAO (Hurrell, 1996; Dima et al., 2001) and, it is in agreement with the relationship identified between winter PC2 and AO/NAO.

The composite map of winter anomalies of Z850 and W850 (Figure 5c) based on the selected PC3 values is characterized by a center of positive Z850 anomalies centered over the British Isle, which is flanked by negative anomalies. The composite of winter SST anomalies (Figure 5f) is characterized by negative anomalies along the eastern coast of US which extend over the central North Atlantic Ocean. Positive SST anomalies emerge in the southern Greenland and in the tropical Atlantic Ocean, while negative SST anomalies extend over the North Sea and the Mediterranean Sea. Such patterns, in the Z850 and SST fields, enhance the advection of cold and dry air (see the wind vectors in Figure 5c) from the North Sea (negative SST anomalies over this area) towards the western part of Europe (where the highest negative loadings of EOF3 of SPEI3 were identified,

406 Figure 1c) favoring dry conditions over these regions. These results are in line with the findings of
407 Madden and Williams (1977) showing that during winter months, cold and dry air has the tendency
408 to suppress precipitation, especially over the European continent.
409
410 **4.2 Spring**

411 High values of spring PC1 coefficients are associated with a wave train of Z850 anomalies (Figure
412 6a) characterized by positive Z850 anomalies over the Greenland, North America, Northern Russia,
413 the Iberian Peninsula and the northern part of Africa and, negative Z850 anomalies centered over the
414 Scandinavian Peninsula. This pattern resembles the negative phase of the spring SCA pattern
415 (Barnston and Livezey, 1987), supporting the high correlation coefficient between the time series of
416 spring PC1 of SPEI3 and spring SCA index (r = -0.42, 99% significance level, Table 3). Positive
417 values of spring PC1 coefficients are associated with positive SST anomalies all over the Atlantic
418 Ocean, with only few exceptions over the Gulf of Mexico, offshore of the eastern US coast and over
419 the Greenland-Irminger-Norwegian (GIN) Sea (negative SST anomalies). Positive SST anomalies
420 extend over the tropical Pacific, Atlantic and Indian oceans (Figure 6d). The cyclonic center over the
421 Scandinavian Peninsula favors the advection of warm and moist air from the Atlantic (positive SST
422 anomalies in Figure 6d) towards most of the European continent (see the wind vectors in Figure 6a)
423 and hence enhances precipitation over these regions. This result is also in line with the EOF1 pattern
424 of spring SPEI3 (Fig 2a) which presents positive loadings over the Scandinavian and most part of
425 Europe.
426 The composite map of spring anomalies of Z850 and W850 (Figure 6b) based on the PC2 values
427 fulfilling the selection criteria is characterized by an extended area of positive Z850 anomalies over
428 the North Atlantic Ocean and most of the Europe, with two centers, one located over the eastern
429 coast of US and the other located over the central Europe and Mediterranean. Negative Z850
430 anomalies cover the Greenland, North Pole and the surrounding areas. This pattern resembles the
431 positive phase of the AO/NAO. As shown in section 3.2, the time series of spring PC2 coefficients
432 and the time series of spring AO/NAO indices are significantly correlated (Table 3). The positive
433 phase of AO is characterized by warmer and wetter than normal conditions over the Scandinavia and
434 northern Russia and colder and drier than normal conditions over the southern part of Europe. These
435 results are also in agreement with the spring pattern of EOF2 of SPEI3 (Figure 2b). The composite
436 of spring SST anomalies associated to PC2 coefficients fulfilling the selection criteria (Figure 6e) is
437 characterized by a tripole-like pattern, with altering signs of SST anomalies in the North Atlantic,

similar to those corresponding to the positive phase of AO (Dima et al., 2001). Both the composites of Z850(W850) and SST anomalies associated with high values of spring PC2 coefficients are similar to the composites of Z850 (W850) and SST anomalies associated to high values of winter PC2, implying a certain persistence from winter to spring of the driving factors and the climate anomalies that are associated to them.

The composite map of spring anomalies of Z850 and W850 (Figure 6c) based on the PC3 values fulfilling the selection criteria (Figure 6c) shows a tripole-like structure between the central North Atlantic Ocean (negative anomalies), the British Isle and Western Europe (positive anomalies) and eastern and south-eastern Europe and western Russia (negative anomalies). This spatial pattern projects onto the positive phase of the Atlantic Multidecadal Oscillation and, it is associated with reduced precipitation over the central Europe (Sutton and Dong, 2012) which is in agreement with the negative loading of the spring EOF3 of SPEI3 (Figure 2c) identified over this regions. Moreover, the dominant feature of the composite map of spring SST anomalies based on PC3 selected values (Figure 6f) is the quasi-monopolar positive anomalies in the North Atlantic Ocean. As indicated by other studies (Latif et al., 2004; Knight et al. 2005) such a quasi-monopolar structure is associated with the extreme phases of the Atlantic Multidecadal Oscillation (AMO). This result is also certified by the correlation coefficient between the time series of spring PC3 coefficients and the time series of spring AMO index (r = 0.37, 99% significance level, *Table 3*) suggesting that the AMO could play an important role in driving moisture variability over Europe. Positive (negative) SST anomalies over the North Atlantic are associated with positive (negative) phase of AMO which induce to dry (wet) conditions over the western Europe and wet (dry) conditions over the eastern Europe and western Russia as also confirmed by the spring EOF3 loadings of SPEI3 (Figure 2c).

4.3 Summer

The composite map of summer anomalies of Z850 and W850 (Figure 7a) based on the PC1 values fulfilling the selection criteria presents a large area of negative anomalies centered over Scandinavia and the British Isles which extends westward over the North Atlantic and the eastern US. Another center of positive anomalies is located over Greenland and adjacent areas, while another area of positive anomalies, centered over the Mediterranean extends eastward to Eurasia. The composite map of summer SST anomalies associated to positive values of PC1 values fulfilling the selection criteria shows negative SST anomalies over the North Sea and along the western coast of Scandinavia and positive SST anomalies along the southern coast of Greenland, central and tropical

Atlantic Ocean and over the Mediterranean Sea. Such patterns, in the summer Z850 and SST anomaly fields, enhance precipitation over the northern and central part of Europe through the advection of warm and moist air (see the wind vectors in Figure 7a) from the central North Atlantic (positive SST anomalies) and inhibit precipitation over the southern part of Europe through the advection of warm and dry air from the northern part of Africa. Moreover, the positive SST anomalies in the Mediterranean Sea and Indian Ocean were found to trigger very dry summers over the southern part of Europe (Hoerling et al., 2012), which is in agreement with our findings.

Positive values of summer the PC2 values fulfilling the selection criteria are associated with a blocking-like pattern in the field of Z850 anomalies, extending over the central and Eastern Europe (Figure 7b). The composite map of Z850 and W850 anomalies also shows two centers of cyclonic circulation, one over Iceland and the Scandinavian Peninsula and another one over the northern Africa. Such a kind of pattern was associated with central and eastern European droughts and heat waves during summer (Cassou et al., 2005; Fisher et al., 2007a). The composite map of summer SST anomalies based on selected PC2 coefficient values is shown in Figure 7e. It presents a quasi-monopolar structure in the North Atlantic with positive SST anomalies over the entire North Atlantic, except some insignificant negative anomalies south-east of Greenland.

The composite map of summer anomalies of Z850 and W850 based on PC3 values fulfilling the selection criteria (Figure 7c) resembles a stationary wave-train pattern with positive anomalies over the central North Atlantic Ocean, Greenland, Scandinavian Peninsula and north-western Russia and a large area of negative anomalies over the British Isle, whole Europe and Eurasia. This pattern is responsible for wet conditions over Europe and dry conditions over Scandinavia and western Russia during summer. The wave-train pattern in the Z850 anomaly field is associated with strong positive SST anomalies in the northern part of the North Atlantic Ocean and GIN Sea (Figure 7f) and negative SST anomalies along the western European coast, the Mediterranean Sea and eastern North America coast. The negative SST anomalies over the Mediterranean Sea and the western European coast could induce wet summers over the central and eastern part of Europe, in agreement with the cyclonic circulation over most of Europe and the British Isles, through the advection of cold and moist air from the eastern coast of the North Atlantic Ocean (see the wind vectors in Figure 7c).

4.4 Autumn

During autumn, high values of PC1 time series of coefficients of SPEI3 fulfilling the selection criteria for building the composite maps are associated with a center of strong negative Z850

anomalies located over the Scandinavian Peninsula and north-western Europe which extends up to central and eastern Europe (Figure 8a). This area of Z850 negative anomalies is surrounded by a large area of positive anomalies extended over the Greenland and Kara Sea, central North Atlantic and northern Africa, Middle East and Eurasia (Figure 8a). This pattern results in a strong pressure gradient between the centers of action, with the highest gradient over the north-western part of Europe. Positive values of autumn PC1 coefficients fulfilling the selection criteria are also associated with negative SST anomalies along the eastern US coast and the western European coast which extend up to the north-western African coast and, an area of negative SST anomalies in the center of North Pacific Ocean (Figure 8a). The composite map of the autumn SST anomalies associated with selected coefficients of the PC1 fulfilling the criteria is characterized by positive SST anomalies in the central North Atlantic extending northward up to the southern Greenland. Outside these areas the SST anomalies are almost insignificant. A similar SST pattern was found to influence the streamflow variability of Rhine River in autumn (Ionita et al., 2012b) and can be obtained by applying an EOF analysis over the autumn SST anomalies over the North Atlantic region and retaining the fourth leading EOF. The atmospheric circulation anomalies and the SST anomalies identified and presented in Figures 8a and d, respectively, favor the advection of moist air, and hence increased precipitation, towards the central part of Europe while the advection of dry air from the northern part of Africa towards the southern part of Europe turns out in reduced precipitation over these regions (see the wind vectors in Figure 8a).

The composite map of autumn Z850 anomalies based on the selected PC2 coefficients points out on a large area of positive anomalies with two centers, one over the north-eastern US coast and the other over the southern Europe. Negative Z850 anomalies associated with a cyclonic circulation are centered northward of Scandinavia and extend over the northern part of the North Atlantic Ocean and Greenland (Figure 8b). This pattern projects onto the positive phase of autumn NAO, which is also in agreement with the significant correlation between the time series of autumn PC2 of SPEI3 and the time series of autumn NAO and AO indices (r = 0.37/0.52, 99% significant level, T*able 3*). The composite map of the autumn SST anomalies based on selected PC2 coefficients (Figure 8e) is characterized by negative SST anomalies around Iceland and tropical Atlantic and Pacific Oceans, and positive SST anomalies over the central North Atlantic off shore the eastern US and western European coasts, and the Mediterranean Sea. A warm Mediterranean Sea favors dry conditions over the southern and south-eastern Europe while the cold North Sea is associated with wetter conditions over the Scandinavian Peninsula and Great Britain.

The composite map of autumn Z850 and W850 anomalies associated to selected PC3 coefficients fulfilling the selection criteria shows a wave train pattern characterized by a sequence of centers of positive and negative Z850 anomalies: one center of negative anomalies over the central Atlantic Ocean, one center of positive anomalies located over the British Isle and western Europe which is connected with another center of positive anomalies located over the Mediterranean and northern Africa and, a center of strong negative anomalies located over the north-western Russia (Figure 8c). This pattern resembles the negative phase of the autumn SCA pattern, which was found to be significantly correlated with the time series of autumn PC3 of SPEI3 (r = -0.39, Table 3). The composite map of the autumn SST anomalies associated to the selected PC3 coefficients presents positive SST anomalies along the eastern US and western European coast and negative SST anomalies over the central North Atlantic Ocean and the Mediterranean Sea (Figure 8f). Such a pattern of SST anomalies could drive/induce dry conditions over the central Europe and wet conditions over the Eastern Europe during autumn.

5. Relationship with Rainday Counts, Cloud Cover and Soil Moisture

In this section the relationship between the seasonal SPEI3 variability and three fields of climatological variables which are rainday counts (WET), cloud cover (CLD) and soil moisture (SOIL) is analyzed in terms of correlation maps between the first three PCs for each season and WET, CLD and SOIL fields. The results of the correlation analysis are shown in Figures 9 – 12, in which the correlations that are exceeding the 95% significance level are hatched.

An increase in air temperature associated with reduced precipitation, which are the main factors driving the drought conditions, can be the result of reductions of cloudiness, especially during spring and summer (Tang et al., 2010). The increase in temperature (which is an important input variable in the computation of SPEI) could also be enhanced by soil moisture reduction, which in turn reduces the evaporation and evaporative cooling on the surface. However, during the winter months positive temperature anomalies are associated with enhanced precipitation, due to the fact that the water holding capacity of the atmosphere limits precipitation amounts during cold conditions (Trenberth and Shea, 2005).

Soil moisture information has the potential to play an important role in predicting the occurrence of drought phenomena and to improve the seasonal prediction of precipitation (Dirmeyer and Brubaker, 1999; Reichle and Koster, 2003). The influence of soil moisture has been studied especially regarding the pre-conditioning in the context of heat waves and summer droughts (Zampieri et al.,

2009; Seneviratne et al., 2006; Fisher et al., 2007b). Moreover, a strong relationship between droughts and cloud cover has been identified, periods of high drought occurrence being associated with a strong decrease in the total cloud amount (Greene et al., 2011). A positive feedback between soil moisture, cloudiness and precipitation has been also reported (Schär et al., 1999; Pal and Eltahir, 2001). A decrease in precipitation triggers dry soil conditions, which in turn would decrease the amount of moist static energy in the boundary layer and an increase in the cloud base height. Such a feedback mechanism would further lead to a decrease in the frequency of convective events, thus reducing the cloud cover and precipitation.

5.1 Winter

Figure 9 presents the correlation maps between the first three winter PCs time series of coefficients and the seasonally averaged rainday counts (left panels), cloud cover (middle panels) and soil moisture (right panels). Winter PC1 is significantly correlated (positive values) with WET (Figure 9a) and SOIL (Figure 9g) over most of the European region. The correlation map between winter PC1 and CLD shows the highest correlations (positive values) over the central and eastern part of Europe, but the correlation coefficients, though significant at 95%, are smaller compared to WET and SOIL. This might be the result of the snow cover influence during winter over these regions. During winter, these regions are more prone to precipitation fallen as snow which is a limiting factor for the heat flux exchange between the surface and the overlying air while the cloud cover role is diminished. Moreover, cloud cover may have a strong impact on suppressing evapotranspiration (Mudiare, 1985). During winter, the evapotranspiration is reduced and hence the CLD effect on SPEI3 variability is smaller compared to WET and SOIL. When analyzing the correlation patterns of winter WET, CLD and SOIL fields presented in Figures 9a, 9d and 9g we can argue that dry (wet) conditions in winter, over most of the European region are the result of a combined effect of WET and SOIL and to a smaller extent to CLD. The correlation maps between the PC2 time series of coefficients of winter SPEI3 and WET, CLD and SOIL fields are shown in Figures 9b, 9e and 9h, respectively. The correlation map between winter PC2 and WET (Figure 9b) presents a dipole-like pattern in the correlation field between the southern part of Europe (negative and significant correlations) and the Scandinavian Peninsula and northern Europe and western Russia (positive and significant correlations). Winter PC2 of SPEI3 is positively correlated with CLD over the western Russia and negatively correlated with CLD over the southern part of Europe (Figure 9e). Comparatively to WET, the values of correlation coefficients between winter PC2 and CLD are

much smaller. The pattern of the correlation map between winter PC2 and SOIL (Figure 9h) is much alike with the WET correlation map (Figure 9b) and with the pattern of winter EOF2 (Figure 1b). As in the case of PC1, WET and SOIL show a higher influence on moisture conditions compared to CLD and, we speculate that this result can be attributed to the direct effect of snow cover. Moisture conditions over the southern part of Europe are sensitive to WET, CLD and SOIL, while over the Scandinavian Peninsula they are more sensitive to WET and SOIL and less sensitive to CLD. In the case of PC3 time series of coefficients, the correlation maps with WET (Figure 9c) and SOIL (Figure 9i) show a similar pattern of correlation characterized by negative correlations over the Iberian Peninsula, British Isle and southern Scandinavian Peninsula and positive correlations over the eastern Europe and Russia which is in agreement with the pattern of winter EOF3 of SPEI3 (Figure 1c). The correlation map between winter PC3 time series of coefficients and CLD (Figure 9f) is different compared to WET and SOIL and shows strong and significant negative correlation over the northern Europe, western Russia and the southern part of the Scandinavian Peninsula. This difference can be due to complex large-scale and regional factors that influence moisture conditions. One of the reason for which the correlation with CLD is smaller in winter can be due to the fact that SPEI3 is based on potential evapotranspiration (PET) and, it was reported that PET is sensitive to CLD mainly in spring and summer (Tang et al., 2010, Ionita et al., 2012c).

5.2 Spring

During spring, the PC1 time series of coefficients is significantly correlated with the WET field (significant and positive correlations up to ~ 0.7) over large areas including the central and northern part of Europe, western Russia and the Scandinavian Peninsula (Figure 10a) and negatively correlated over the Iberian Peninsula, southernmost part of Europe and the Middle East. The correlation map between spring PC1 and spring CLD (Figure 10d) is similar to the correlation map of WET (Figure 10a) but the correlation coefficients are smaller compared to WET, though still significant. Dry (wet) conditions over the central and western part of Europe and western Russia are associated with decreased (increased) soil moisture content over these regions. The correlation map for SOIL also shows a low negative correlation along the western and northern coast of the Scandinavian Peninsula. This aspect may be due to the fact that the western coast of Scandinavian Peninsula is a mountain region and most of the soils are formed on glacial materials (Jones et al., 2005) and the bedrock is calcareous, this characteristic making these soils less sensitive to moisture. The correlation maps between the spring PC2 series of coefficients and spring WET (Figure 10b),

spring CLD (Figure 10e) and spring SOIL (Figure 10h) present similar correlation patterns. Dry (wet) conditions over the southern and central part of Europe (the Scandinavian Peninsula) are associated with reduced (enhanced) rainday counts (Figure 10b), low (high) cloudiness (Figure 10e) and decreased (increased) soil moisture content (Figure 10h). In the case of spring PC2 all three considered parameters (WET, CLD and SOIL) seem to play an important role on determining dryness/wetness conditions over the analyzed regions, in terms of correlation coefficients. Figures 10c, 10f and 10i present the correlation maps between the spring PC3 time series of coefficients and WET field (Figure 10c), CLD field (Figure 10f) and SOIL field (Figure 10i). The regions exhibiting the highest correlations between spring PC3 and WET (Figure 10c), CLD (Figure 10f) and SOIL (Figure 10i) are the Eastern Europe and western Russia (positive correlations) and Western Europe (negative correlations). Dry (wet) conditions over the western Russia and Eastern Europe are associated with decreased (increased) rainday counts, low (high) cloudiness and reduced (enhanced) soil moisture content over these regions. As in the case of the winter season, the correlation between the spring PCs and spring CLD were smaller compared to spring WET and spring SOIL, especially over the northern part of Europe (areas which in spring can still be covered by snow, Brown and Robinson, 2011). Again, we can speculate that these results can be an effect of the influence of snow cover, which acts as a barrier between the surface layer and the overlying air.

5.3 Summer

Figures 11a, 11d and 11g present the correlation maps between the summer PC1 time series of coefficients and the summer WET, CLD and SOIL fields. The correlation patterns show a dipole-like structure, with the highest positive correlations over the northern part of Europe, western Russia and the Scandinavian Peninsula and negative correlations over the southern part of Europe. The magnitudes of the correlation coefficients are almost the same for all three analyzed fields (WET, CLD and SOIL). Wet (dry) conditions over the northern part of Europe, Scandinavian Peninsula and western part of Russia are associated with enhanced (reduced) rainday counts (Figure 11a), high (low) cloudiness (Figure 11d) and increased (decreased) soil moisture content (Figure 11g) over these regions. For the southern part of Europe dry (wet) conditions are associated with reduced (enhanced) rainday counts, low (high) cloudiness and decreased (increased) soil moisture content. The correlation map of summer PC2 with WET (Figure 11b) and CLD (Figure 11e) fields shows the highest negative (positive) correlations over western Russia (Scandinavian Peninsula, Western Europe and Turkey), while in the case of SOIL field, the correlation map shows significant negative

correlations over western Russia and positive correlations only over small regions (Turkey and northern part of Sweden). This is not surprisingly, since the highest negative loadings of summer EOF2 are found over western Russia. Therefore, enhanced (reduced) rainday counts, high (low) cloudiness and increased (decreased) soil moisture anomalies lead to wet (dry) periods over most of the western part of Russia. The correlation coefficients between summer PC3 series of coefficients with WET, CLD and SOIL fields are positive and significant over most of continental part of Europe and southern Scandinavian Peninsula. Over the north-western part of Russia the correlation is negative. In terms of correlation coefficients values the influence of CLD and SOIL on moisture conditions over the north-western part of Russia is much smaller compared to WET. Tang et al. (2012) showed that over this region the summer temperature (which is an integrated part in the definition of SPEI) is more sensitive to precipitation variability than to cloud cover and, this could also explain the highest correlation between summer PC3 and WET over north-western Russia.

5.4 Autumn

Figures 12a, 12d and 12g show the correlation maps between the autumn PC1 time series of coefficients and the autumn WET, CLD and SOIL fields, respectively. The correlation maps show a pattern of positive (negative) correlation with the highest positive significant values centered over the northern part of Europe, the Scandinavian Peninsula and western part of Russia (southern part of Europe). The highest correlations are found between the autumn PC1 time series and WET and SOIL (Figures 12a and 12g, respectively). The autumn PC2 time series of coefficients is negatively correlated with WET (Figure 12b), CLD (Figure 12f) and SOIL (Figure 12h) over most of the part of Europe and positively correlated with WET and SOIL over the Scandinavian Peninsula and northern Russia. The correlation maps between the PC3 time series of coefficients and seasonally averaged WET, CLD and SOIL are presented in Figures 12c, 12f and 12i, respectively. They are very similar in the spatial distribution of correlation coefficients though the highest correlation coefficients are recorded between the autumn PC3 and WET (Figure 12c). Dry (wet) conditions over the western part of Europe are associated with reduced (enhanced) rainday counts, low (high) cloudiness and decreased (increased) soil moisture anomalies. At the same time, wet (dry) conditions over the western part of Russia are associated with enhanced (reduced) rainday counts, high (low) cloudiness and increased (decreased) soil moisture content. As in the case of summer, the correlation coefficients between the autumn PC3 time series of SPEI3 and WET and SOIL is stronger compared to CLD.

6. Discussion

As a complex natural hazard, drought is best characterized by multiple climatological and hydrological parameters, therefore is very important to understand the association of drought with climatic, oceanic and local factors. Persistent dry (wet) conditions are usually associated with persistent anticyclones (cyclones) (Schubert et al., 2014), while the sea surface temperature plays also an important role on dryness and wetness variability, via large scale climate modes of variability (e.g. AMO and/or ENSO) (Ionita et al., 2012a).

In this study the spatio-temporal variability of the seasonal short-term dryness and wetness conditions as represented by SPEI3 over the European region are investigated, and the relationship with large-scale factors is highlighted. There are relatively few studies that assess this relationship and most of them are either restricted to areas prone to drought (Iberian Peninsula, Mediterranean region or the southern part of Europe) or to a particular season (mostly summer). A strong relationship between the seasonal variability of temperature and precipitation, which are key factors in driving the dryness and wetness conditions, and the global atmospheric circulation, has already been reported (Hurrell et al., 1995; Slonosky et al., 2001; Zveryaev et al., 2006, 2009; Sutton and Hodson, 2005). The aim of this study is to provide more insights on the seasonal dryness/wetness variability over the European region based on the analysis of SPEI3 which is an index that quantifies the moisture status based on temperature and precipitation.

During the winter season the variability of SPEI3 was found to be linked to well-known climate modes: AO/NAO, SCA, EAWR and EA. Moreover, in our study we showed that the combined effect of these climate modes (NAO vs. SCA and EAWR), not just NAO, may have quite a strong impact on SPEI3 variability. This is a very important result, especially in the view of the recent findings of Comas-Bru and McDermott (2013), who showed that the NAO centers of actions are influence by the phase of the SCA and the EA patterns. Although NAO is one of the most prominent teleconnection patterns in all seasons (Barnston and Livezey, 1987), its relative role in regulating the variability of the European climate during non-winter months is not that clear as for the winter season. At the same time, the mechanisms which drive the European climate variability might vary from one climatic period to another and, also, they might be different for different variables (e.g. precipitation, streamflow, air temperature and drought).

The winters PCs series of coefficients are associated with cyclonic (anticyclonic) circulations over the regions where the corresponding EOFs have the highest positive (negative) loadings. According to the composite maps of Z850, W850 and SST anomalies based on the selected values of winter

PC1, the cyclonic circulation is associated with the advection of warm air from the Atlantic Ocean (positive SST anomalies) and with higher rainday counts and higher cloudiness, which in turn are responsible for the wet periods over these regions. The winter PC1 of SPEI3 was found to be more correlated with winter WET and SOIL than with CLD. Reduced (enhanced) rainday counts together with decreased (increased) soil moisture content contribute to a higher degree to drought variability during winter compared to low (high) cloud cover. The influence of the cloud cover can be diminished by the presence of snow cover, which can limit the heat flux exchange between the surface and the overlying air.

As in the case of winter season, dryness and wetness variability during spring is strongly related to climatic modes of variability. The leading mode of spring variability of SPEI3 is positively correlated with the EA mode and negatively correlated with POL and SCA modes. According to the second mode of spring variability of SPEI3, dry (wet) conditions over the central and southern part of Europe (Scandinavian Peninsula) are associated with an atmospheric circulation mode that projects onto the positive phase of AO/NAO modes. Also, the spring PC2 time series of coefficients is negatively correlated with the SCA mode. The spring PC3 time series of coefficients of SPEI3 is positively correlated with AMO and negatively correlated with NAO and SCA. AMO was found to play an important role in the modulation of the European climate, especially during summer (Sutton and Hodson, 2005; Ionita et al., 2013). Recent studies showed that AMO can modulate the climate variability over Europe also during the transition seasons (Ionita et al., 2012c; Sutton and Dong, 2012). In general, high values of SPEI3 were associated with positive anomalies of rainday counts; cloud cover and soil moisture content over the regions were the highest positive loadings are found in the EOF maps. The highest correlation of spring PCs time series of coefficients was identified with the WET field compared with CLD and SOIL. Nevertheless, CLD and SOIL plays also a significant role in spring dryness and wetness variability, but the correlations, though significant, are smaller compared to WET field.

The pattern of the first mode of SPEI3 variability over Europe during summer is also the result of the influence of various teleconnection patterns. The summer PC1 of SPEI3 is negatively correlated with the NAO/AO, EAWR and SCA, and positively correlated with the EA. The influence of these large scale teleconnection modes resulted in a spatial distribution of the Z850 anomalies in a wave train pattern characterized by a center of positive anomalies over Greenland, a center of negative anomalies over the central North Atlantic extending up to the Scandinavian Peninsula and another center of positive anomalies over the Mediterranean Sea extending up to central Russia. Such kind

of circulation pattern favors the advection of warm and dry air from the northern part of Africa towards the southern part of Europe (see the wind vectors in the composite maps), which in turn will experience dry conditions. It is well known that the atmospheric circulation during summer seasons is mostly influenced by the atmospheric blocking as it was shown in the composite map of Z850 anomalies associated to PC2 series of coefficients. Most of the extreme events related to heat waves in Europe, during summer, were triggered by such a particular atmospheric pattern. Anomalously barotropic structures are particularly strong (weak) in June (July) when the large scale anomalies are organized in wave trains that propagate from the Atlantic Ocean towards the European continent (Xopalki et al., 1995; Corte-Real et al., 1995; Cassou et al., 2005). Summer dry conditions over western Russia are associated with a blocking like pattern over Europe It is characterized by an anticyclonic circulation over the eastern part of Europe and two centers of cyclonic circulation, one over the Scandinavian Peninsula and the British Isles, and another one over the northern part of Africa. Such a pattern of atmospheric blocking was responsible for one of the most extreme summer heat waves recorded over the eastern Europe and Russia during 2010 (Dole et al., 2011). In general, the atmospheric blocking in summer is associated with extreme temperatures and heat waves (Della-Marta et al., 2007, Garcia-Herrera et al., 2010; Feudale and Shukla, 2010). During summer, the correlation maps of PCs time series of coefficients with WET, CLD and SOIL show similar patterns (in terms of amplitude of the correlation coefficients) but the strength and the significance of the correlation coefficients demonstrate that the WET and SOIL fields have more influence on moisture variability than CLD.

The first mode of autumn moisture variability was found to be significantly correlated with the autumn POL and EAWR teleconnection patterns. The second mode of autumn moisture variability is strongly related to AO/NAO modes, as in the case of winter EOF2. Dry (wet) conditions over central and the southern part of Europe (Scandinavian Peninsula) are associated with Z850 and SST anomalies that project onto the positive phase of AO/NAO. The third mode of the autumn variability of SPEI3 is the result of the influence of various teleconnection patterns. The PC3 is positively correlated with NAO/AO and negatively correlated with SCA. The composite of Z850 anomalies based on selected PC3 values presents a wave train pattern (with altering signs) which develops over the Atlantic Ocean and extends up to Siberia. Higher correlations have been identified between the autumn PCs and WET and SOIL fields compared to CLD.

7. Conclusions

The mains conclusions of our study can be summarized as follows:

- The leading modes of SPEI3 variability are definitely seasonally – dependent. Although the spatial structure of the leading modes of seasonal variability of SPEI3 may show resemblance between each other, the temporal evolution (in terms of principal component time series of coefficients) differs significantly from one season to another. Moreover, the leading modes of dryness and wetness variability quantified by SPEI3 are associated with particular atmospheric circulation patterns and sea surface temperature anomalies for each season. The analysis of seasonal composite maps of Z850, W850 and global SST anomalies and of seasonal correlation maps of the first three PCs of SPEI3 and WET, CLD and SOIL fields pointed out on a specific and significant role of each of these climatic variables on the seasonal short-term SPEI3 variability.
- The response of dryness/wetness variability quantified by SPEI3 to SST anomalies was found to be more regional during summer, compared to other seasons. This might be due to the fact that during summer moisture conditions are more sensitive to local conditions (e.g. precipitation, soil moisture). Another reason might be that the response of air temperature over the land (which is an input parameter for the computation of SPEI) to SST anomaly variations is seasonally dependent and, this seasonality is mainly due to the warming trends of SST (Cattiaux et al., 2010).
- Overall, the correlation maps between the PC time series of coefficients corresponding to the three leading modes of seasonal SPEI3 variability and the fields of WET, CLD and SOIL show much similarities with the patterns of EOF loadings, meaning that the regions with the highest loadings in the EOF field are similar to the regions where the highest correlation is recorded in the correlation maps of the seasonal PCs with WET, CLD and SOIL fields. The main difference arises from the fact that in some seasons and for particular regions WET and SOIL show stronger influence (in terms of correlation coefficient amplitude) on dryness/wetness conditions over Europe compared to CLD. This might be one of the direct results of the fact that the SPEI3 variability is modulated both by local and large scale-factors. The differences in the correlation maps between seasonal PCs and WET, CLD and SOIL fields might also be due to the different soil types that characterize different regions. One specific example is the western part of the Scandinavian Peninsula, where the effect of soil moisture is less that important due to the fact that the soils over these regions mainly

consist of glacial materials (which are not sensitive to soil moisture, Jones et al., 2005).

- The findings of this paper also suggest that dryness and wetness variability over Europe is influenced by rainday counts, cloud cover and soil moisture as a direct result of atmospheric circulation anomalies. The physical mechanisms involved in dryness/wetness variability are very complex and differ from one season to another. Precipitation deficits can be induced by various processes including decreasing cloudiness, and land surface drying can slack evapotranspiration and thus inhibiting cloud formation. This can be the result of the direct effect of atmospheric factors (e.g. cyclones and anticyclones) and global and/or regional SST anomalies. Moreover, when studying the variability of the moisture in connection to large scale circulation, one should take into account the soil characteristics to specific regions.

The main findings of this study are that the leading EOF modes of SPEI3 variability are characterized by seasonal differences and, their relationship with the large-scale atmospheric circulation, global SST, rainday counts, cloud cover and soil moisture is also seasonal - dependent. The results presented here also point out on how complex the drivers of the dryness and wetness variability at the European scale are. Given the complex nature of seasonal dryness/wetness variability and the temporal scales of its potential impact on various socio-economic sectors, a next logical step will be to perform a similar analysis for mid-range and long-term dryness and wetness variability quantified with SPEI.

Acknowledgements. The work was supported by the REKLIM (Regionale Klimaänderungen/ Regional climate change) project and Polar Regions and Coasts in a changing Earth System Project (PACES II).

881 # References

882

883 Alley WM (1984) The Palmer drought severity index: Limitations and applications. J Appl Meteor
884 23:1100–1109

885 Barnston AG, Livezey RE (1987) Classification, seasonality, and persistence of low-frequency
886 atmospheric circulation patterns. Mon Wea Rev 115:1083–1126

887 Boroneant, C, Potop V, Mozný M, Štepánek P, Skalák P (2012) Large scale circulation patterns
888 associated to seasonal dry and wet conditions over the Czech Republic. pp. 271-280 in
889 Cambio climático. Extremos e impactos. Publicaciones de la Asociación Española de
890 Climatología (AEC), 2012, Serie A, n. 8, Salamanca, 998 pp. ISBN: 978-84-695-4331-3.

891 Briffa KR, G. van der Schrier G, Jones PD (2009) Wet and dry summers in Europe since 1750:
892 evidence of increasing drought. Int J Climatology 29: 1894-190.

893 Brown, R. D. and Robinson, D. A.: Northern Hemisphere spring snow cover variability and change
894 over 1922–2010 including an assessment of uncertainty, The Cryosphere, 5, 219-229,
895 doi:10.5194/tc-5-219-2011, 2011.

896 Cai W, Cowan T (2008) Evidence of impacts from rising temperature on inflows to the Murray-
897 Darling Basin. Geophys Res Lett 35: L07701 doi:10.1029/2008GL033390

898 Cassou C, Terray L, Phillips A (2005) Tropical Atlantic influence on European heat waves. J
899 Climate 18: 2011–2805

900 Cattiaux J., Vautard R, Yiou P (2010) North-Atlantic SST amplified recent wintertime European
901 land temperature extremes and trends. Clim Dyn 36(11–12): 2113–2128 doi:
902 10.1007/s00382-010-0869-0

903 Comas-Bru L, McDermott F (2013) Impacts of the EA and SCA patterns on the European twentieth
904 century NAO–winter climate relationship. QJR Meteorol Soc in press doi: 10.1002/qj.2158

905 Compo GP, Whitaker JS, Sardeshmukh PD (2006) Feasibility of a 100 year reanalysis using only
906 surface pressure data. Bull Amer Met Soc 87:175-190

907 Compo GP, Whitaker JS, Sardeshmukh PD, Matsui N, Allan RJ, Yin X, Gleason BE, Vose RS,
908 Rutledge G, Bessemoulin P, Brönnimann S, Brunet M, Crouthamel RI, Grant AN, Groisman
909 PY, Jones PD, Kruk M, Kruger AC, Marshall GJ, Maugeri M, Mok HY, NordlI Ø, Ross TF,

910 Trigo RM, Wang XL, Woodruff SD, Worley SJ(2011) The Twentieth Century Reanalysis
911 Project. QJR Meteorol Soc 137: 1-28. DOI: 10.1002/qj.776.
912 Corte-Real J, Zhang X, Wang X(1995) Large-scale circulation regimes and surface climatic
913 anomalies over the Mediterranean. Int J Climatol 15: 1135–1150
914 Dai A (2011a) Drought under global warming: a review. Wiley Interdiscip Rev Clim Chang 2:45–65
915 Dai A (2011b) Characteristics and trends in various forms of the Palmer Drought Severity Index
916 during 1900–2008. J Geophys Re, 116: D12115 doi:10.1029/2010JD015541
917 Della-Marta PM, Haylock MR, Luterbacher J, Wanner H (2007) Doubled length of western
918 European summer heat waves since 1880. J Geophys Res 112:D15103
919 Dima M, Rimbu N, Stefan S, Dima I (2001) Quasi-Decadal Variability in the Atlantic Basin
920 Involving Tropics–Midlatitudes and Ocean–Atmosphere Interactions. J Climate **14:** 823–832.
921 Dirmeyer PA, Brubaker KL (1999) Contrasting evaporative moisture sources during the drought of
922 1988 and the flood of 1993. J Geophys Res 104(D16): 19383–19397
923 *doi:*10.1029/1999JD900222
924 Dole R, Hoerling M, Perlwitz J, Eischeid J, Pegion P, Zhang T, Quan XW, Xu T, Murray D (2011)
925 Was there a basis for anticipating the 2010 Russian heat wave? Geophys Res Lett 38:
926 L06702 *doi:*10.1029/2010GL046582

927 Enfield DB, Mestas-Nuñez AM, Trimble PJ (2001) The Atlantic Multidecadal Oscillation and its
928 relation to rainfall and river flows in the continental US. Geophys Res Lett 28: 2077–2080
929 Estrela MJ, Penarrocha D, Millan M (2000) Multi-annual drought episodes in the Mediterranean
930 (Valencia region) from 1950–1996. A spatio-temporal analysis. Int J Climatol 20:1599–1618
931 Farago T, Kozma E, Nemes C (1989) Drought indices in meteorology. Idojaras 93(1): 45–59
932 Feudale L, Shukla J (2010) Influence of sea surface temperature on the European heat wave of 2003
933 summer. Part I: An observational study. Clim Dyn 36: 1691–703
934 Fischer EM, Seneviratne SI, Vidale PL, Lüthi D, Schär C (2007a) Soil moisture–atmosphere
935 interactions during the 2003 European summer heat wave. J Climate 20: 5081–99
936 Fischer EM, Seneviratne SI, Lüthi D, Schär C (2007b) Contribution of land atmosphere coupling to
937 recent European summer heat waves. Geophys Res Lett 34: L06707
938 doi:10.1029/2006GL029068.
939 Folland CK, Karl TR, Christy JR, Clarke RA, Gruza GV, Jouzel J, Mann ME, Oerlemans J,
940 Salinger JM, Wang SW (2001) Observed climate variability and change. In Climate change
941 2001: The scientific basis. Contribution of Working Group I to the Third Assessment Report

942 of the Intergovernmental Panel on Climate Change, ed. J. T. Houghton, Y. Ding, D. J.
943 Griggs,M. Noguer, P. J. van der Linden, X. Dai, K.Maskell, and C.A. Johnson, 881.
944 Cambridge: Cambridge University Press.
945 Garcia-Herrera R, Diaz J, Trigo RM, Luterbacher J, Fischer EM (2010) A review of the European
946 summer heat wave of 2003. Critical Reviews in Environmental Science and Technology 40:
947 267-306
948 Greene H, Leighton HG, Stewart RE (2011) Drought and Associated Cloud Fields over the
949 Canadian Prairie Provinces. Atmosphere-Ocean 49 (4): 356-365
950 Harris I, Jones PD, Osborn TJ, Lister DH (2013) Updated high-resolution grids of monthly climatic
951 observations. In press Int J Climatol Doi: 10.1002/joc.3711
952 Heim RR (2002) A review of twentieth-century drought indices used in the United States. Bull Am
953 Meteorol Soc 83(8):1149–1165
954 Hurrel JW (1995) Decadal Trends in the North Atlantic Oscillation Regional Temperatures and
955 Precipitation. Science 269: 676–679
956 Hurrell JW (1996) Influence of variations in extratropical wintertime teleconnections on Northern
957 Hemisphere temperature. Geophys Res Lett 23: 665–668
958 Ionita M, Lohmann G, Rimbu N (2008) Prediction of Elbe discharge based on stable teleconnections
959 with winter global temperature and precipitation. J Climate 21: 6215-6226.
960 DOI:10.1175/2008JCLI2248.1

961 Ionita M, Rimbu N, Lohmann G (2011) Decadal variability of the Elbe River streamflow. Int J
962 Climatol 31 22–30 doi: 10.1002/joc.2054
963 Ionita M, Lohmann G, Rimbu N, Chelcea S, Dima M (2012a) Interannual to decadal summer
964 drought variability over Europe and its relationship to global sea surface temperature. Clim
965 Dyn 38(1–2):363–377
966 Ionita M, Lohmann G, Rimbu N, Chelcea S (2012b) Interannual Variability of Rhine River
967 Streamflow and Its Relationship with Large-Scale Anomaly Patterns in Spring and Autumn.
968 J Hydrometeor **13**: 172–188

969 Ionita M, Lohmann G, Rimbu N, Scholz P (2012c) Dominant modes of Diurnal Temperature Range
970 variability over Europe and their relationships with large-scale atmospheric circulation and
971 sea surface temperature anomaly patterns. J Geophys Res doi:10.1029/2011JD016669 in
972 press

973 Ionita M, Rimbu N, Chelcea S, Patrut S (2013) Multidecadal variability of summer temperature over
974 Romania and its relation with Atlantic Multidecadal Oscillation. Theor and Appl Clim
975 113:305–315

976 Jones, R.J.A., Houšková, B., Bullock P. and Montanarella L. (eds) 2005. Soil Resources of Europe,
977 second edition. European Soil Bureau Research Report No.9, EUR 20559 EN, 420pp. Office
978 for Official Publications of the European Communities, Luxembourg
979 Jones PD, Moberg A (2003) Hemispheric and Large-Scale Surface Air Temperature Variations: An
980 Extensive Revision and an Update to 2001. J Climate 16: 206–223

981 Knight JR, Allan RJ, Folland CK, Vellinga M, Mann ME (2005) A signature of persistent natural
982 thermohaline circulation cycles in observed climate. Geophys Res Lett 32 L20708
983 doi:10.1029/2005GL024233
984 Koleva E, Alexandrov V (2008) Drought in the Bulgarian low regions during the 20th century.
985 Theor Appl Climatol 92:113–120
986 Latif M, Roeckner E, Botzet M, Esch M, Haak H, Hagemann S, Jungclaus J, Legutke S, Marsland S,
987 Mikolajewicz U, Mitchell JFB (2004) Reconstructing, monitoring, and predicting
988 multidecadal-scale changes in the North Atlantic thermohaline circulation with sea surface
989 temperature. J Climate 17: 1605–1614
990 Livada I, Assimakopoulos VD (2007) Spatial and temporal analysis of drought in Greece using the
991 Standardized Precipitation Index (SPI). Theor Appl Climatol 89:143–153
992 Lloyd-Hughes B, Saunders MA (2002) A drought climatology for Europe. Int J Climatol 22:1571–
993 1592

994 Madden R.A., J. Williams, 1978: The Correlation between Temperature and Precipitation in the
995 United States and Europe. *Mon. Wea. Rev.*, **106**, 142–147.

996 Maracchi G (2000) Agricultural drought – a practical approach to definition, assessment and
997 mitigation strategies. In: Vogt JV, Somma F (eds) Drought and drought mitigation in Europe.
998 Advances in Natural and Technological Hazards Research, vol. 14. Kluwer Acad Publ: 63–
999 75
1000 Mariotti A, Zeng N, Lau K-M, (2002) Euro-Mediterranean rainfall and ENSO - a seasonally varying
1001 relationship. Geophys Res Lett 29 (12) 10.1029/2001GL014248

1002 McKee TBN, Doesken J, Kleist J (1993) The relationship of drought frequency and duration to time

1003 scales. Proc Eight Conf on Applied Climatology. Anaheim, CA, Amer. Meteor. Soc. 179–
1004 184

1005 Mesta-Nuñez AM, Enfield DB (1999) Rotated global modes of non-ENSO sea surface temperature
1006 variability. J Climate 12: 2734-2746

1007 Mudiare O (1985) Influence of Light Rainfall Activity and Cloud Cover on Evapotranspiration
1008 Demands. Ph.D. Thesis, University of Saskatchewan, Saskatoon, SK. p. 105.

1009 Nicholls N (2004) The changing nature of Australian droughts. Clim Change 63: 323−326

1010 Pal JS, Eltahir EAB (2001) Pathways relating soil moisture conditions to future summer rainfall
1011 within a model of the land-atmosphere system. J Climate 14: 1227–1242

1012 Palme WC *(*1965) Meteorological Drought. Res Paper No. 45 Weather Bureau Washington D.C. 58
1013 pp.

1014 Ped DA (1975) On parameters of drought and humidity. Papers of the USSSR hydrometeorological
1015 center 156: 19–38 (in Russian)

1016 Potop V., Boroneanţ C., Mozný M., Štepánek P., Skalák P. (2013) Observed spatiotemporal
1017 characteristics of drought on various time scales over the Czech Republic. Theoretical and
1018 Applied Climatology. DOI: 10.1007/s00704-013-0908-y.

1019 Rayner NA, Parker DE, Horton EB, Folland CK, Alexander LV, Rowell DP, Kent EC, Kaplan A
1020 (2003) Globally complete analyses of sea surface temperature, sea ice and night marine air
1021 temperature, 1871-2000. J Geophy Res 108: 4407 doi:10.1029/2002JD002670

1022 Reichle RH,Koster RD (2003) Assessing the Impact of Horizontal Error Correlations in Background
1023 Fields on Soil Moisture Estimation. J Hydrometeor 4: 1229–1242

1024 Rimbu N*,* Dima M*,* Lohmann G*,* Stefan *S (*2004*)* Impacts of the North Atlantic Oscillation and the
1025 El Niño–Southern Oscillation on Danube river flow variability. Geophys Res Lett 31:
1026 *L23203 doi:*10.1029/2004GL020559

1027 Schär, C., Luthi, D., Beyerle, U. and Heise, E. 1999. The soil-precipitation feedback: a process
1028 study with a regional climate model. *J. Clim.*, 12: 722–741.

1029 Schlesinger ME*,* Ramankutty N (1994) An oscillation in the global climate system of period 65–70
1030 years. Nature 367*:* 723–726

1031 Schubert S.D., Hailan Wang, Randal D. Koster, Max J. Suarez, and Pavel Ya. Groisman, 2014:
1032 Northern Eurasian Heat Waves and Droughts. *J. Climate*, **27**, 3169–3207.

1033 Seneviratne SI, Luethi D, Michael L, Schaer C (2006) Land–atmosphere coupling and climate

change in Europe. Nature 443 205–9

Slonosky VC, Jones PD, Davies TD (2001) Atmospheric circulation and surface temperature in Europe from the 18th century to 1995. Int J Climatol 21: 63-75

Solomon S, Qin D, Manning M, Marquis M, Averyt K, Tignor MMB, Miller HL, Chen Z (2007) Climate Change 2007: The Physical Science Basis. Cambridge University Press 996 pp

Sutton RT, Hodson DLR (2005) Atlantic Ocean forcing of North American and European summer climate. Science 309: 115–118

Sutton R, Dong B(2012) Atlantic Ocean influence on a shift in European climate in the 1990s. Nature Geoscience 5 (10): 788–792

Tang Q, Leng G, Groisman PY, 2012: European Hot Summers Associated with a Reduction of Cloudiness. J Climate 25: 3637–3644

Tao, H., Borth, H., Fraedrich, K., Su, B. and Zhu, X. (2014), Drought and wetness variability in the Tarim River Basin and connection to large-scale atmospheric circulation. Int. J. Climatol., 34: 2678–2684. doi: 10.1002/joc.3867

Trnka M, Kysely J, Možný M, Dubrovský M (2009a) Changes in Central-European soil-moisture availability and circulation patterns in 1881–2005. Int J Climatol 29(5):655–672

van Oldenborgh GJ, Burgers G, Klein Tank A (2000) On the El Nino teleconnection to spring precipitation in Europe. Int J Climatol 20: 565–574

Vicente-Serrano SM, Beguería S, López-Moreno JI (2010) A multi-scalar drought index sensitive to global warming: the Standardized Precipitation Evapotranspiration Index—SPEI. J Clim 23(7):1696–1718

Vicente-Serrano SM, López-Moreno JI, Drumond A, Gimeno L and others (2011) Effects of warming processes on droughts and water resources in the NW Iberian Peninsula (1930−2006). Clim Res 48:203-212

Vicente-Serrano SM, Beguería S, López-Moreno JI (2011) Comment on “Characteristics and trends in various forms of the Palmer Drought Severity Index (PDSI) during 1900-2008” by A. Dai. J Geophys Res Lett -Atmosphere 116: D19112 doi:10.1029/2011JD016410

von Storch H, Zwiers FW (1999) Statistical Analysis in Climate Research. Cambridge University Press 494 pp.

1063 Weber L, Nkemdirim LC (1998) The Palmer drought severity index revisited. Geogr Ann 80A:
1064 153–172
1065 Whitaker JS, Compo GP, Wei X, Hamill TM (2004) Reanalysis without radiosondes using ensemble
1066 data assimilation. Mon Wea Rev 132: 1190-1200
1067 Wilhite DA, Glantz MH (1985) Understanding the drought phenomenon: the role of definitions.
1068 Water Int 10: 111–120
1069 World Meteorological Organization (WMO) (1975) Drought and agriculture. WMO/TN 138,
1070 Geneva: WMO 118 pp
1071 Xoplaki E, Gonzalez-Rouco JF, Luterbacher J, Wanner H (2003a) Mediterranean summer air
1072 temperature variability and its connection to the large-scale atmospheric circulation and
1073 SSTs. Clim Dyn 20: 723–739 DOI 10.1007/s00382-003-0304-x
1074 Zampieri M, D'Andrea F, Vautard R, Ciais P, De Noblet-Ducoudré N, Yiou P (2009) Hot European
1075 summers and the role of soil moisture in the propagation of Mediterranean drought. J Clim
1076 22: 4747–58
1077 Zveryaev II, Gulev SK (2009) Seasonality in secular changes and interannual variability of
1078 European air temperature during the twentieth century. J Geophys Res 114: D02110
1079 doi:10.1029/2008JD010624
1080 Zveryaev II *(*2006*)* Seasonally varying modes in long-term variability of European precipitation
1081 during the 20th century. J Geophys Res 111: D21116 doi*:*10.1029/2005JD006821
1082
1083
1084
1085
1086
1087
1088
1089
1090

Figure 1. a) Spatial patterns of the first winter EOF mode of the SPEI3 field; b) Spatial patterns of the second winter EOF mode of the SPEI3 field; c) Spatial patterns of the third winter EOF mode of the SPEI3 field; d) The times series of the first Principal Component (PC1) corresponding to the first winter EOF mode and its corresponding 7-yr running mean (black line); e) The times series of the second Principal Component (PC2) corresponding to the second winter EOF mode and its corresponding 7-yr running mean (black line); f) The times series of the third Principal Component (PC3) corresponding to the third winter EOF mode and its corresponding 7-yr running means (black line).

Figure 2. As in Figure 1, but for Spring.

Figure 3. As in Figure 1, but for Summer.

Figure 4. As in Figure 1, but for Autumn.

Figure 5. a) The composite map (High – Low) between the winter PC1 and winter Z850 (shaded) and the wind vectors at 850mb (arrows); b) As in Figure 5a, but for winter PC2; c) As in Figure 5a, but for winter PC3; d) The composite map (High – Low) between the winter PC1 and global winter SST; e) As in Figure 5d, but for winter PC2; f) As in Figure 5d, but for winter PC3; (The dotted areas indicate the Z500 and SST normalized anomalies significant at 95 % significance level on a standard t-test).

Figure 6. As in Figure 5, but for Spring.

Figure 7. As in Figure 5, but for Summer.

Figure 8. As in Figure 5, but for Autumn.

Figure 9. a) The correlation maps between winter PC1 and winter wet days (WET); b) The correlation maps between winter PC2 and winter wet days (WET); c) The correlation maps between winter PC3 and winter wet days (WET); d) The correlation maps between winter PC1 and winter Cloud Cover (CLD); e) The correlation maps between winter PC2 and winter Cloud Cover (CLD); f) The correlation maps between winter PC3 and winter Cloud Cover (CLD); g) The correlation maps between winter PC1 and winter Soil Moisture (SOIL); h) The correlation maps between winter PC2 and winter Soil Moisture (SOIL); i) The correlation maps between winter PC3 and winter Soil Moisture (SOIL); The dotted areas indicate the areas where the correlation coefficient is significant at 95 % significance level.

Figure 10. As in Figure 9, but for Spring.

Figure 11. As in Figure 9, but for Summer.

Figure 12. As in Figure 9, but for Autumn.

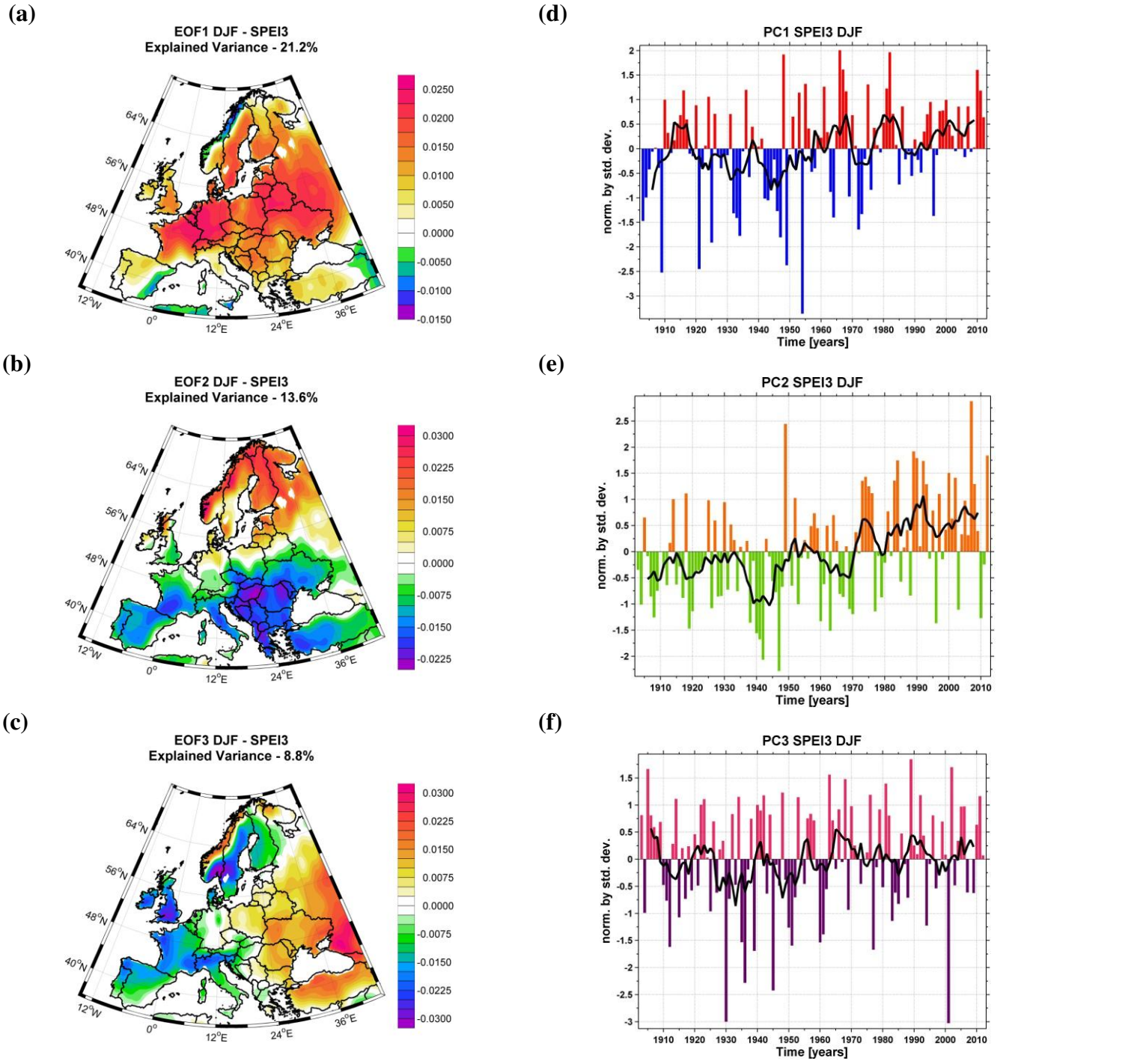

Figure 1. a) Spatial patterns of the first winter EOF mode of the SPEI3 field;
b) Spatial patterns of the second winter EOF mode of the SPEI3 field;
c) Spatial patterns of the third winter EOF mode of the SPEI3 field;
d) The times series of the first Principal Component (PC1) corresponding to the first winter EOF mode and its corresponding 7-yr running mean (black line);
e) The times series of the second Principal Component (PC2) corresponding to the second winter EOF mode and its corresponding 7-yr running mean (black line);
f) The times series of the third Principal Component (PC3) corresponding to the third winter EOF mode and its corresponding 7-yr running means (black line).

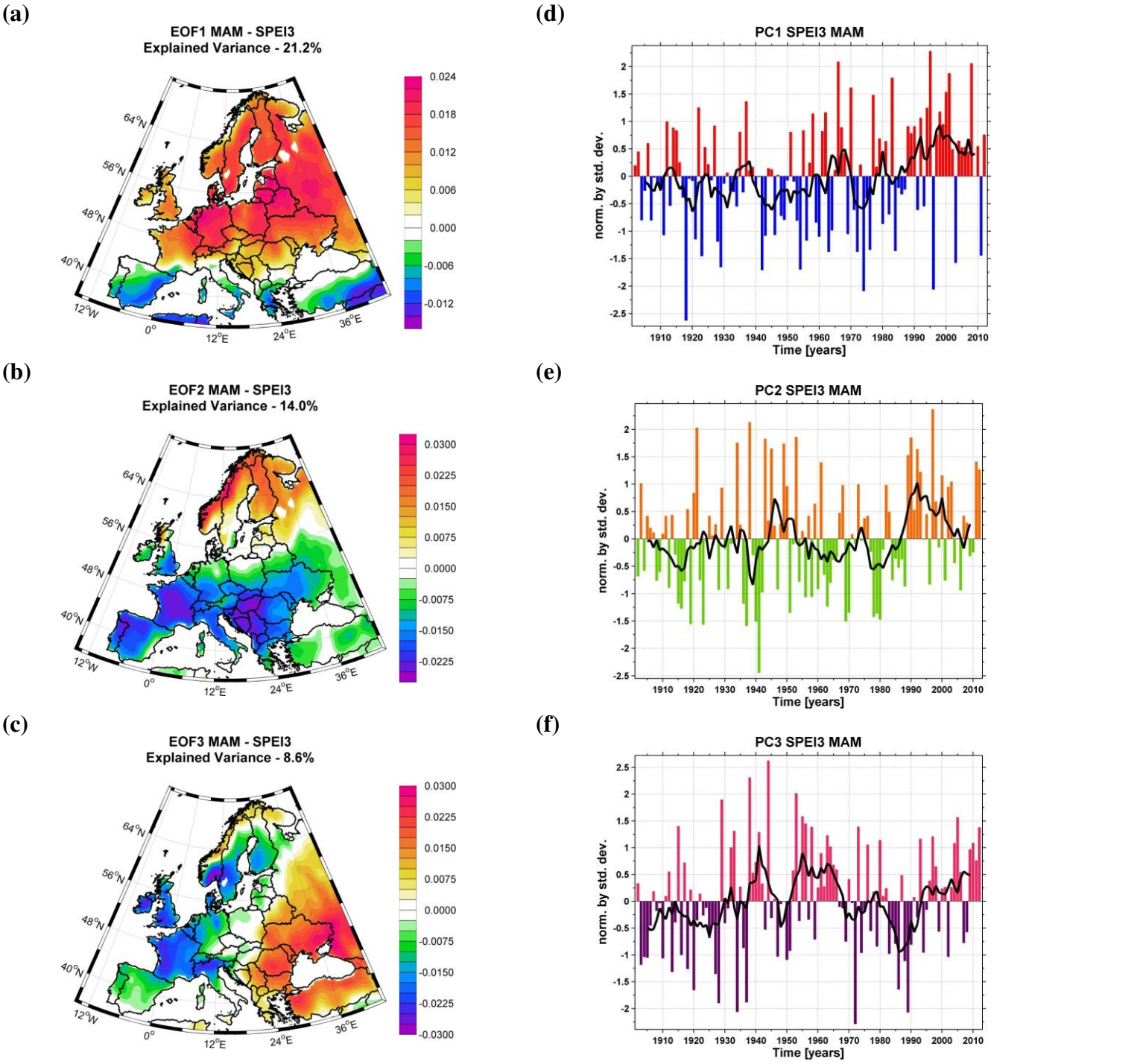

Figure 2. As in Figure 1, but for Spring.

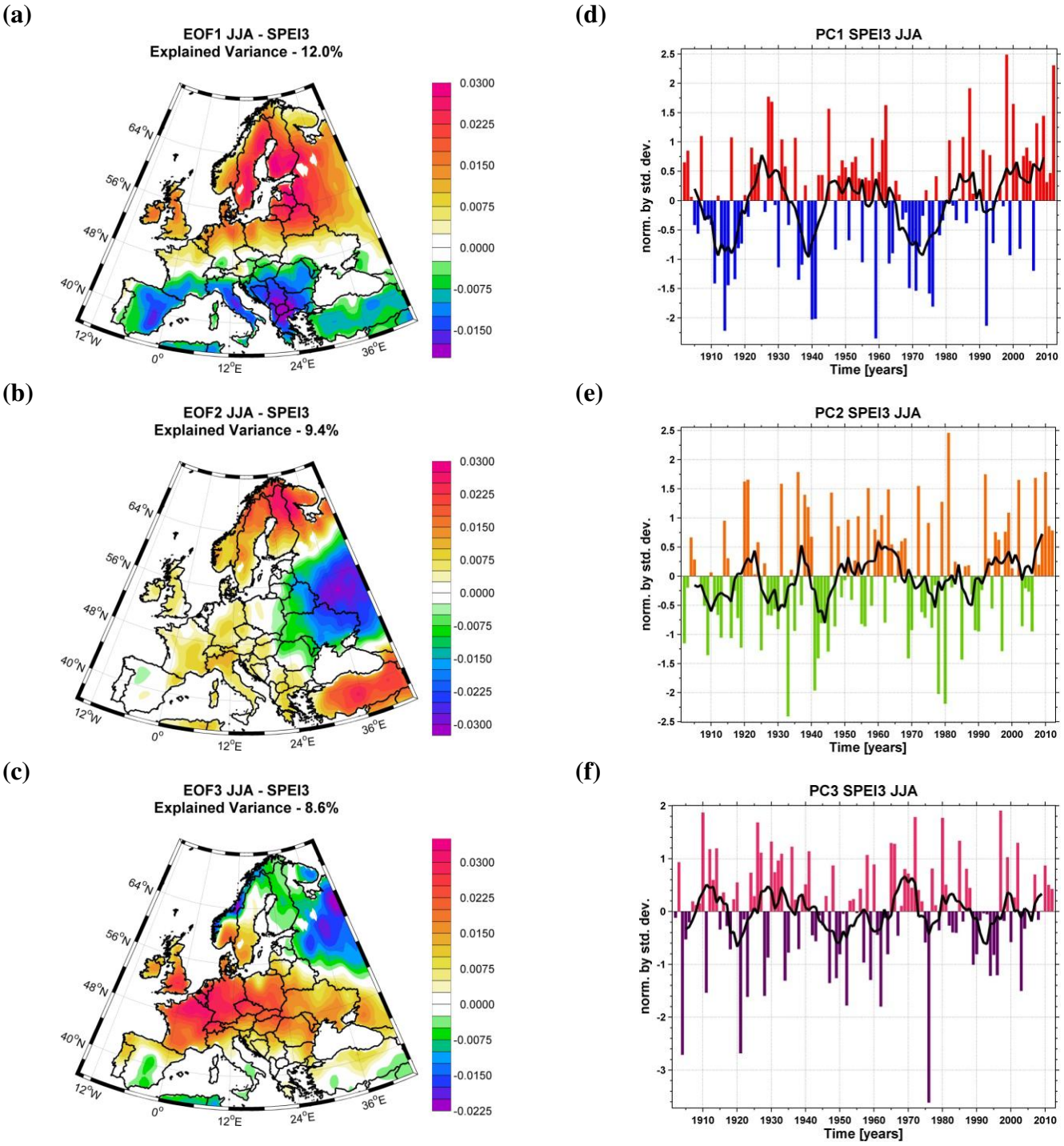

Figure 3. As in Figure 1, but for Summer.

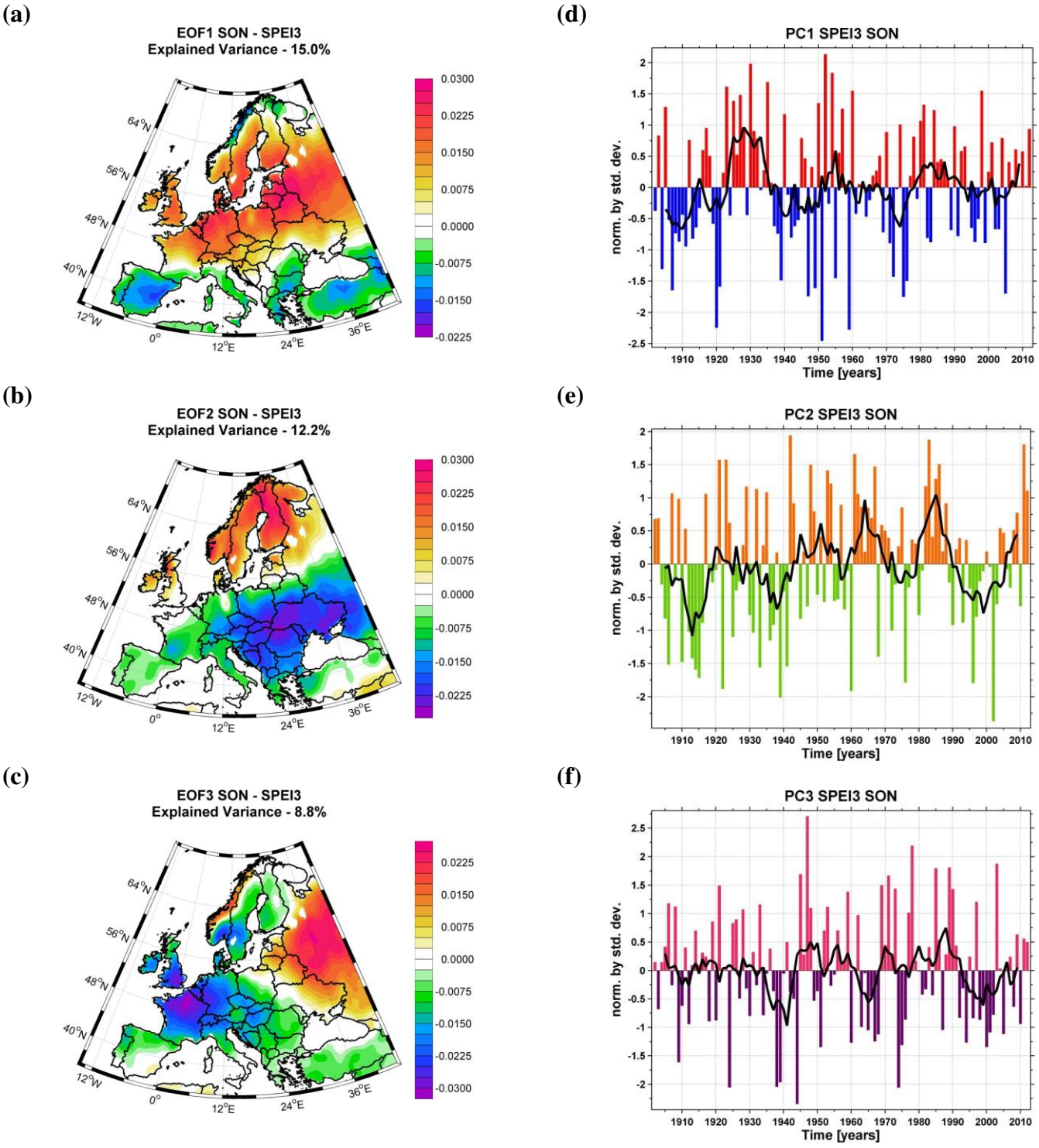

Figure 4. As in Figure 1, but for Autumn.

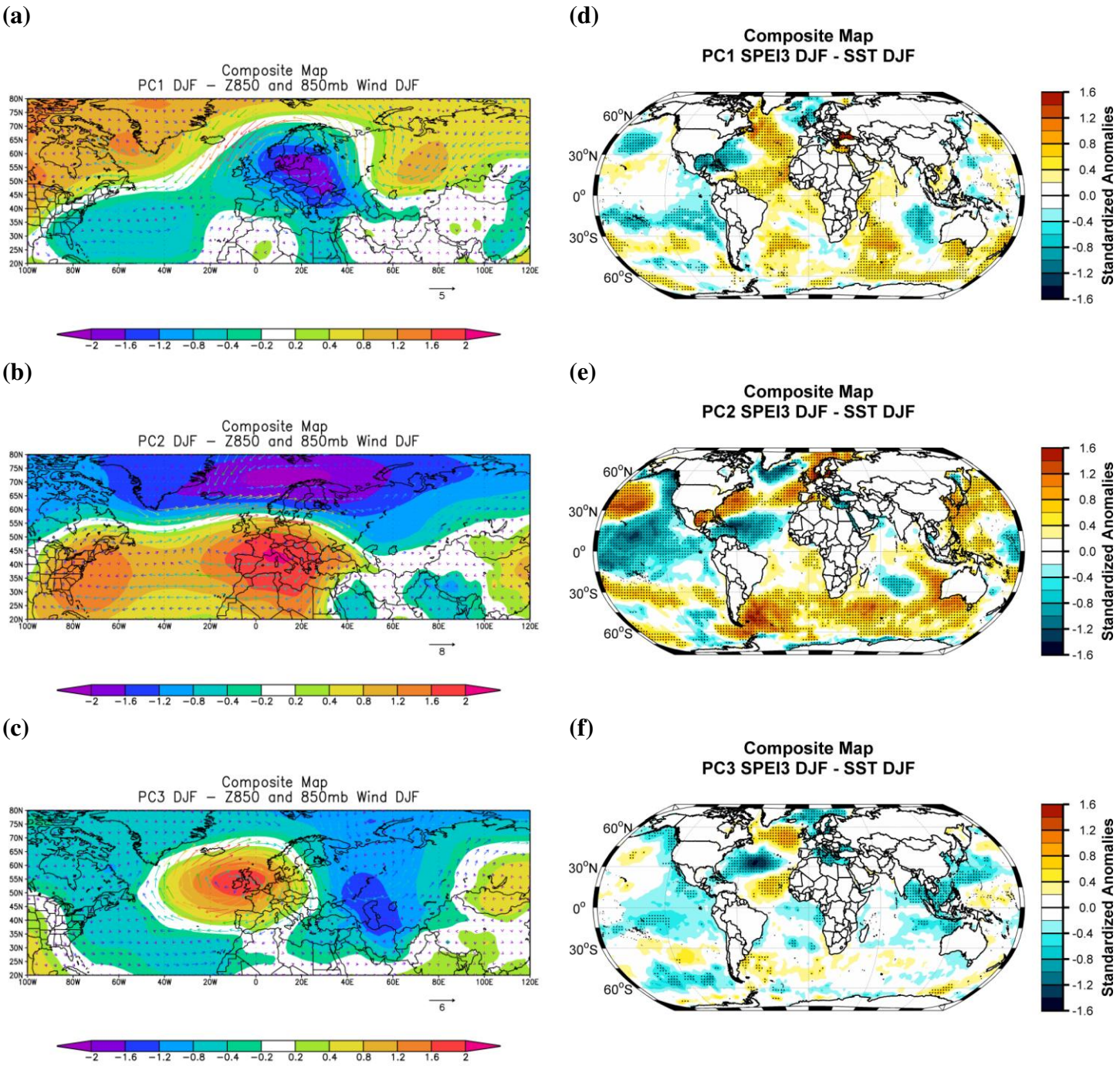

Figure 5. a) The composite map (High – Low) between the winter PC1 and winter Z850 (shaded) and the wind vectors at 850mb (arrows);
b) As in Figure 5a, but for winter PC2;
c) As in Figure 5a, but for winter PC3;
d) The composite map (High – Low) between the winter PC1 and global winter SST;
e) As in Figure 5d, but for winter PC2;
f) As in Figure 5d, but for winter PC3;
(The dotted areas indicate the Z500 and SST normalized anomalies significant at 95 % significance level on a standard t-test).

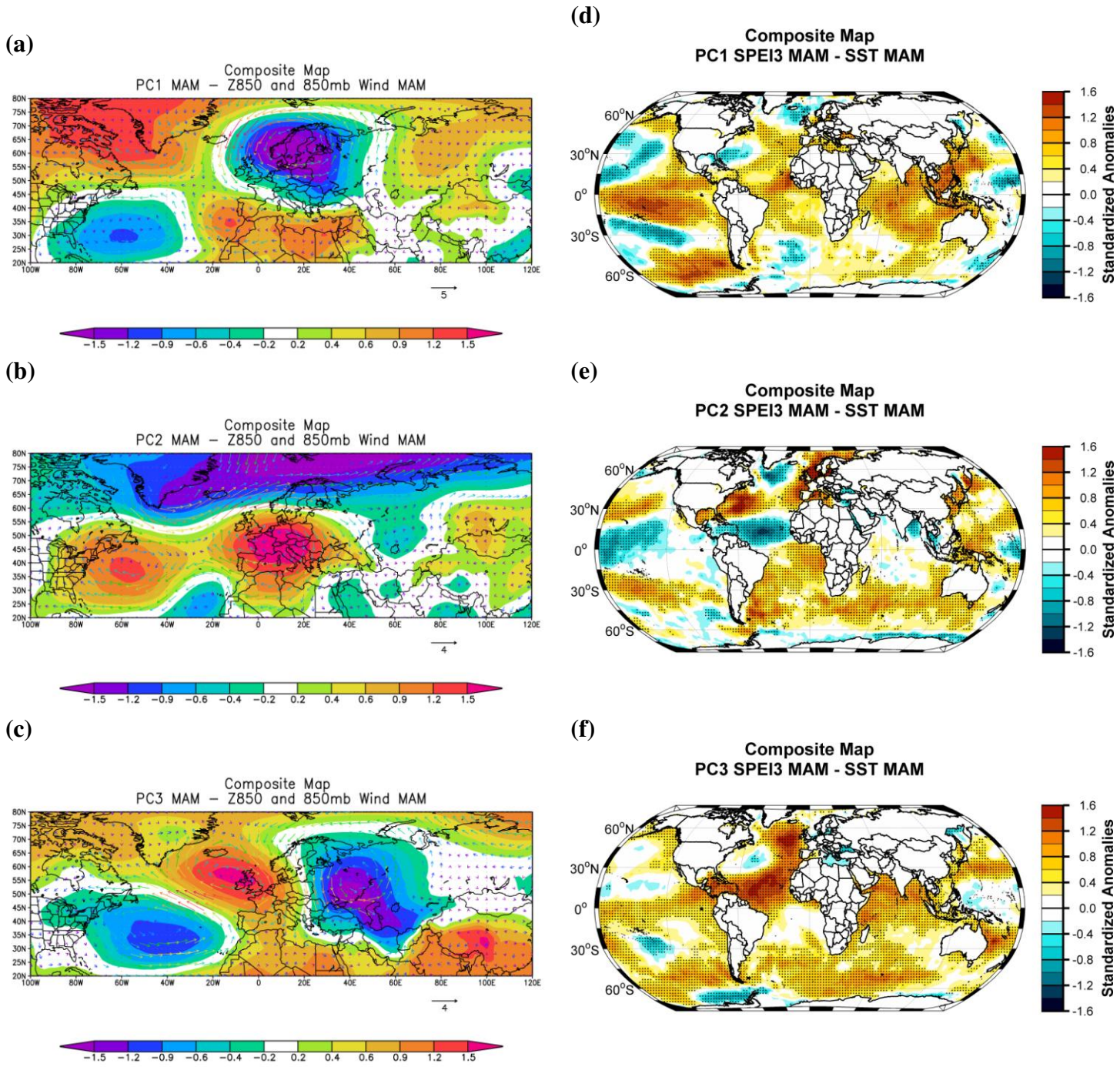

Figure 6. As in Figure 5, but for Spring.

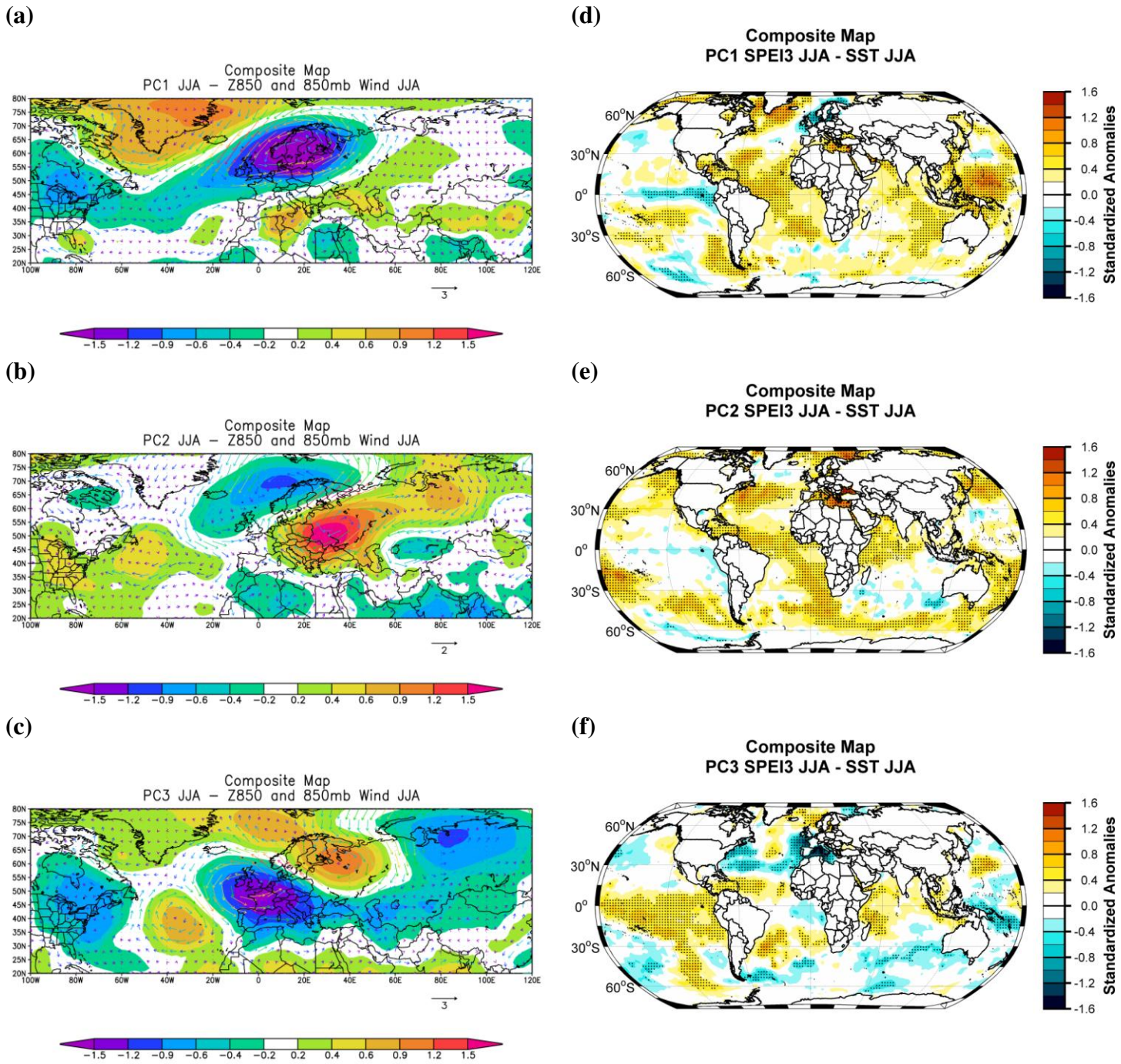

Figure 7. As in Figure 5, but for Summer.

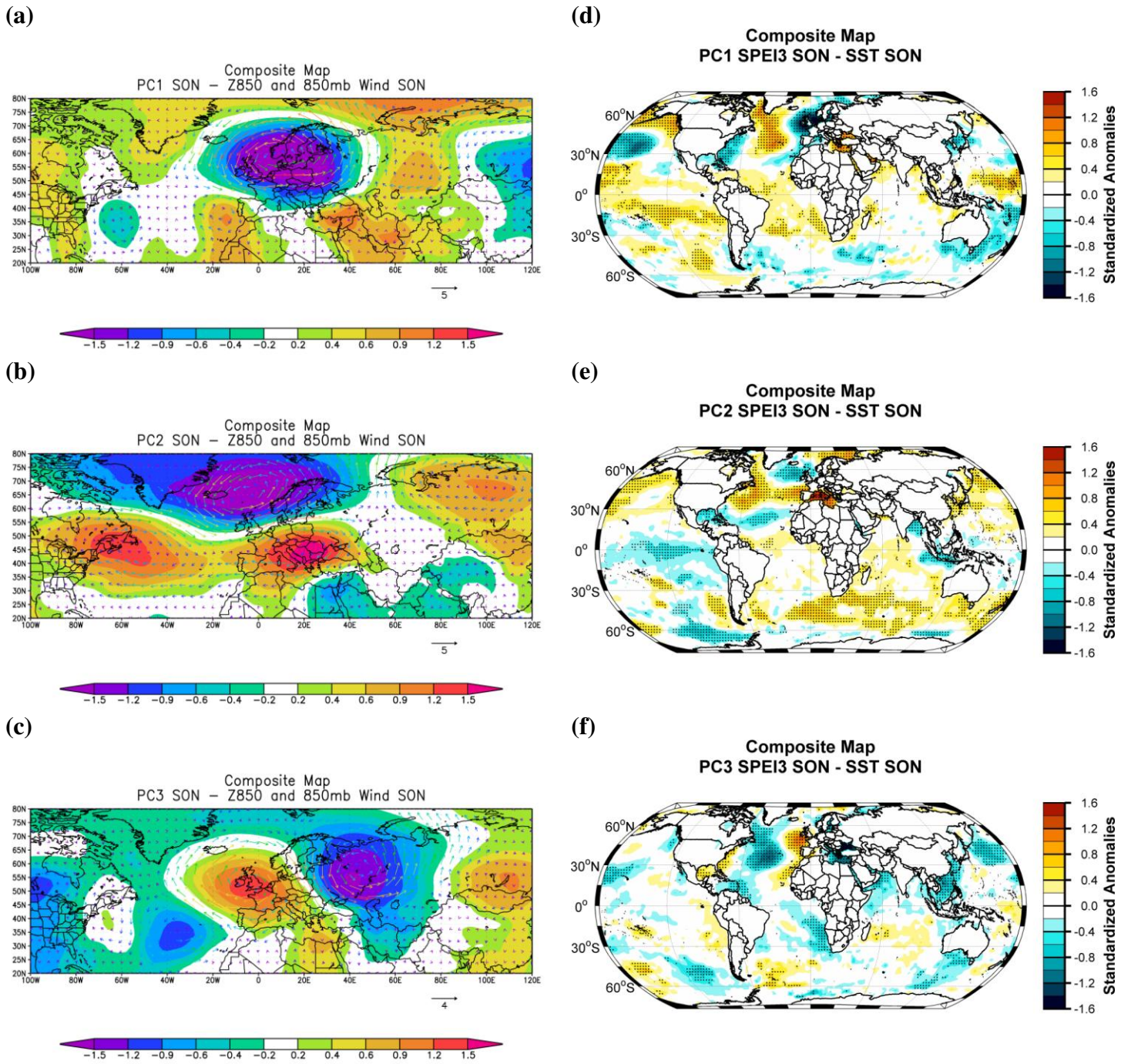

Figure 8. As in Figure 5, but for Autumn.

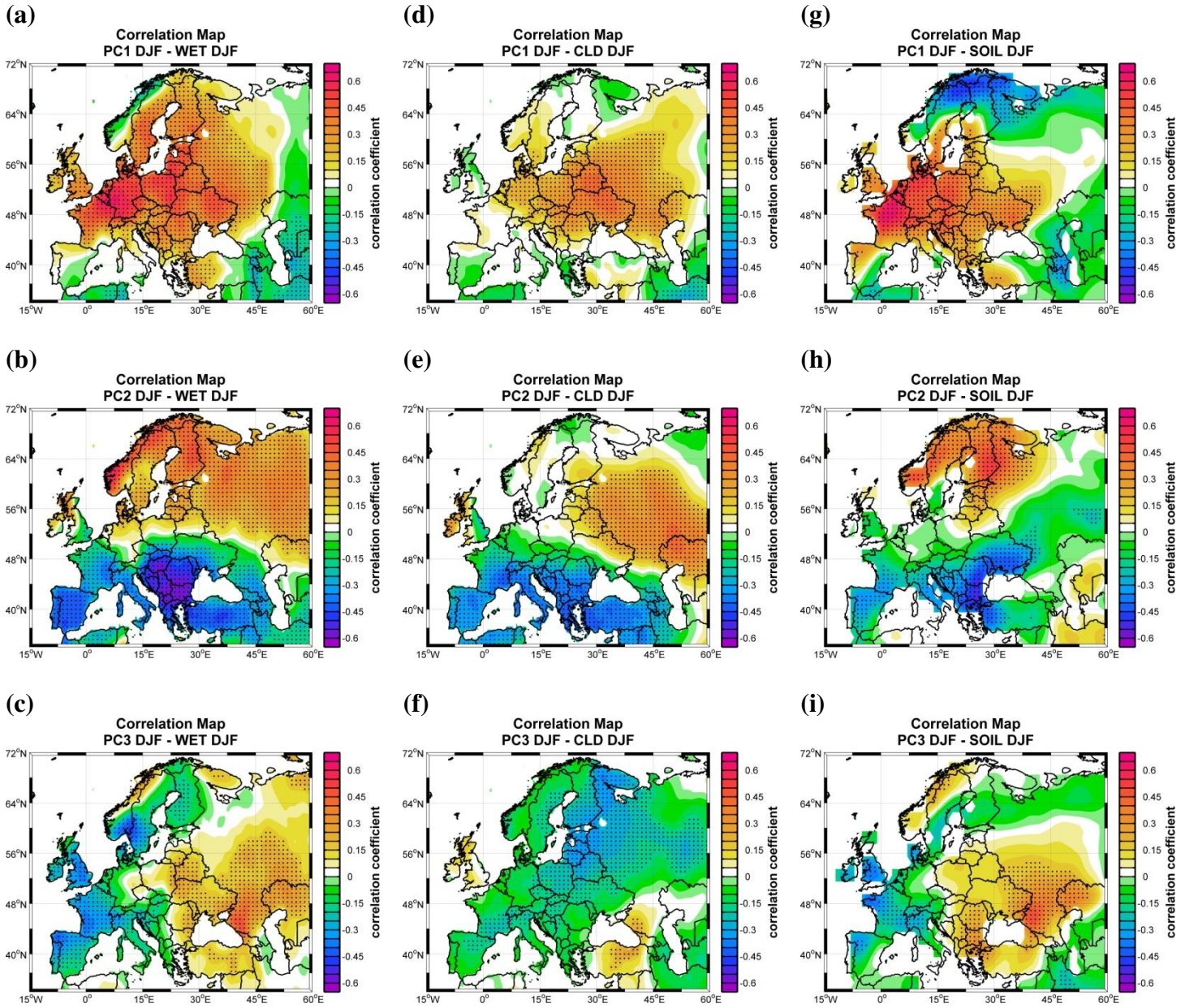

Figure 9. a) The correlation maps between winter PC1 and winter wet days (WET);
b) The correlation maps between winter PC2 and winter wet days (WET);
c) The correlation maps between winter PC3 and winter wet days (WET);
d) The correlation maps between winter PC1 and winter Cloud Cover (CLD);
e) The correlation maps between winter PC2 and winter Cloud Cover (CLD);
f) The correlation maps between winter PC3 and winter Cloud Cover (CLD);
g) The correlation maps between winter PC1 and winter Soil Moisture (SOIL);
h) The correlation maps between winter PC2 and winter Soil Moisture (SOIL);
i) The correlation maps between winter PC3 and winter Soil Moisture (SOIL);
The dotted areas indicate the areas where the correlation coefficient is significant at 95 % significance level.

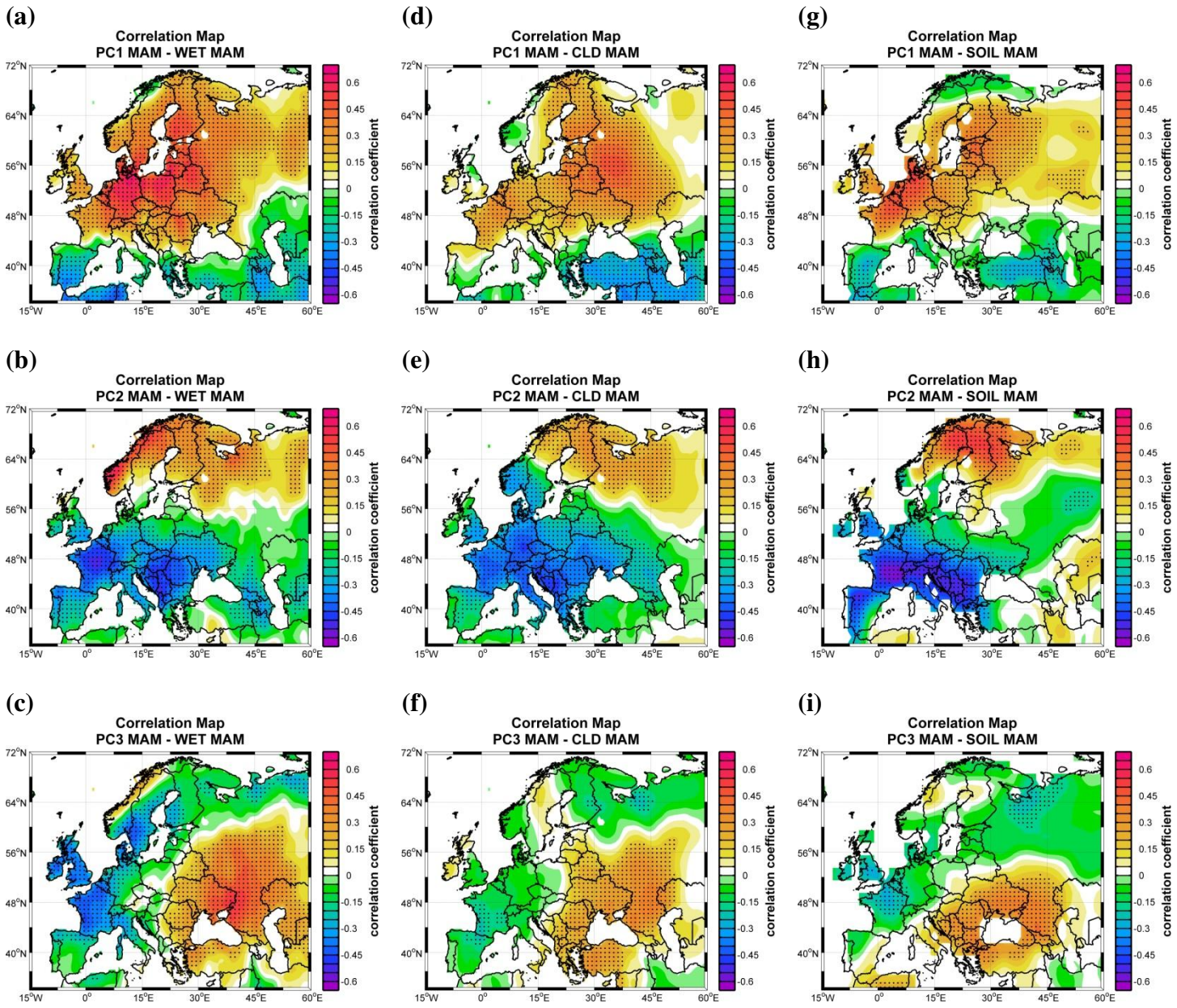

Figure 10. As in Figure 9, but for Spring.

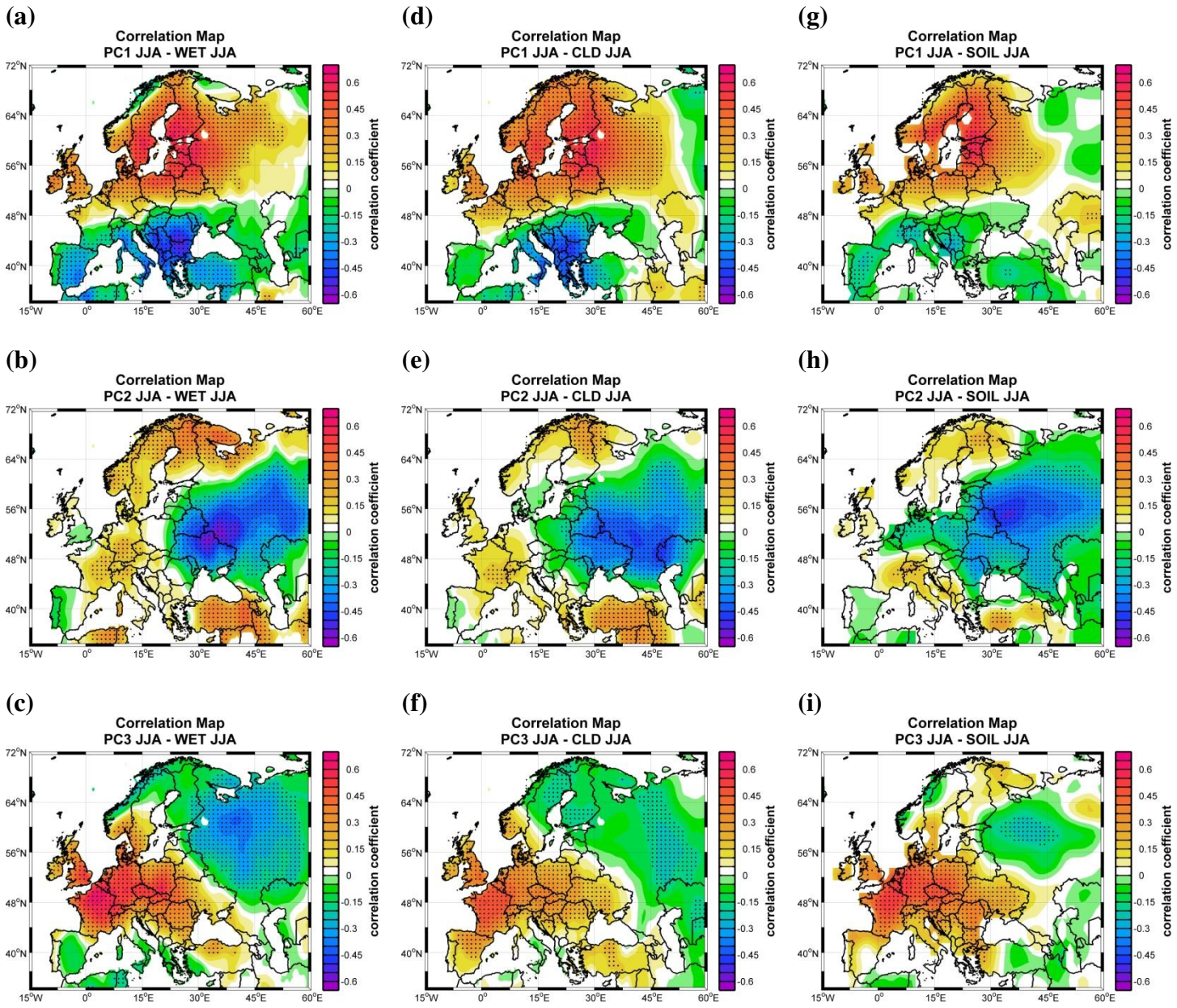

Figure 11. As in Figure 9, but for Summer.

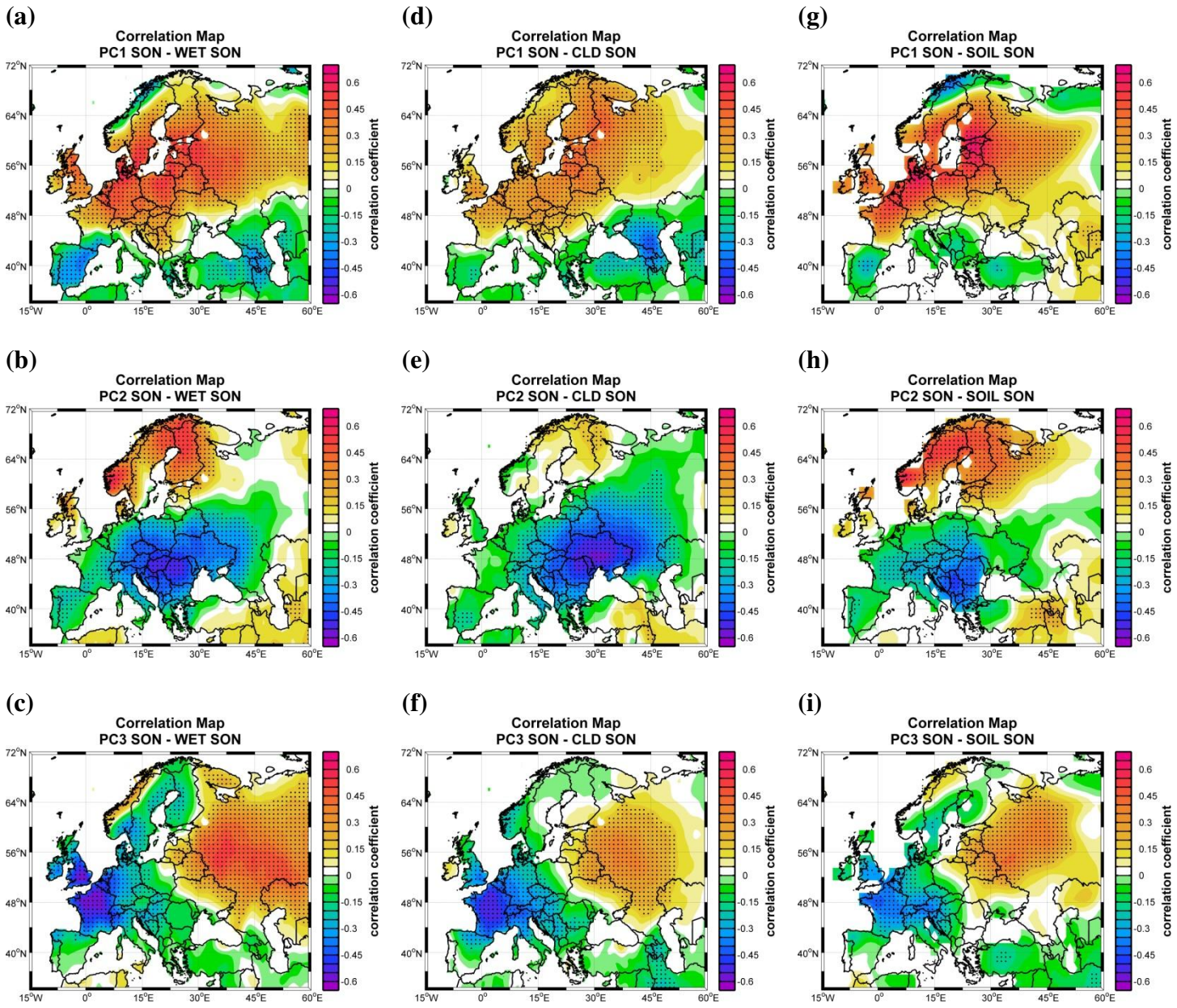

***Figure 12*.** As in Figure 9, but for Autumn.

Table 1. The explained variance of the first ten seasonal EOFs. The EOFs highlighted in red, are the seasonal EOFs used in this study.

Explained variance (%)				
No. EOF	**Winter**	**Spring**	**Summer**	**Autumn**
EOF1	**21.2**	**21.2**	**612.0**	**15.0**
EOF2	**13.6**	**14.0**	**4.69.4**	**12.2**
EOF3	**8.8**	**8.6**	**8.6**	**8.8**
EOF4	5.7	5.1	6.3	6.5
EOF5	4.0	3.8	4.6	4.0
EOF6	3.7	3.0	4.1	3.3
EOF7	3.5	2.9	3.5	3.2
EOF8	3.3	2.0	2.8	2.6
EOF9	2.0	1.9	2.4	2.5
EOF10	1.9	1.8	2.0	2.0

Table 2. Teleconnection indices used in this study, time period and their source

Name	**Explanation**	**Period**	**Data source**
AMO	Atlantic Multidecadal Oscillation	1950-2012	http://climexp.knmi.nl/data/iamo_hadsst2.dat
NAO	North Atlantic Oscillation	1950-2012	http://www.cru.uea.ac.uk/cru/data/nao.htm
AO	Arctic Oscillation	1950-2012	http://www.atmos.colostate.edu/ao/Data/ao_index.html
SCA	Scandinavian Pattern	1950-2012	http://www.cpc.noaa.gov/data/teledoc/scand.shtml
EAWR	East Atlantic/ Western Russia	1950 - 2012	http://www.cpc.ncep.noaa.gov/data/teledoc/eawruss.shtml
EA	East Atlantic	1950 - 2012	http://www.cpc.ncep.noaa.gov/data/teledoc/ea.shtml
Niño 3.4	Niño 3.4 index	1950 - 2012	http://iridl.ldeo.columbia.edu/SOURCES/.Indices/.nino/.KAPLAN/
Niño 4	Niño4 index		http://iridl.ldeo.columbia.edu/SOURCES/.Indices/.nino/.KAPLAN/
POL	Polar/Eurasia	1950 - 2012	http://www.cpc.ncep.noaa.gov/data/teledoc/poleur.shtml
PDO	Pacific Decadal Oscillation	1950 - 2012	http://jisao.washington.edu/pdo/

Table 3. Correlation coefficients between the SPEI 3 Principal Components (PCs) corresponding to the first three seasonal EOFs and the seasonal teleconnection patterns ($^{\#}$ - 90% significance level; * - 95% significance level; ** - 99% significance level).

	PC1				**PC2**				**PC3**			
	DJF	**MAM**	**JJA**	**SON**	**DJF**	**MAM**	**JJA**	**SON**	**DJF**	**MAM**	**JJA**	**SON**
AMO	0.14	0.19	**0.27***	0.15	0.02	0.01	0.01	-0.10	0.03	**0.37****	-0.15	-0.08
AO	-0.17	-0.04	**-0.31****	-0.14	**0.79****	**0.52****	-0.11	**0.52****	0.16	-0.20	**-0.31****	**0.31****
EA	0.18	**0.35****	**0.40****	0.02	0.06	0.08	0.08	0.19	**-0.28***	-0.04	**0.25***	-0.20
EAWR	**-0.24**$^{\#}$	-0.12	**-0.47****	**-0.25***	**0.34****	-0.01	**-0.27***	-0.09	**0.28***	0.12	-0.10	**0.26***
NAO	0.05	-0.16	**-0.55****	-0.19	**0.64****	**0.27***	-0.03	**0.37****	-0.03	**-0.25***	**-0.26***	**0.31****
NINO3.4	0.01	0.19	0.09	-0.15	-0.13	0.11	0.06	-0.09	-0.12	0.18	0.16	0.00
NINO4	0.00	0.12	0.03	-0.04	**-0.22**$^{\#}$	0.01	0.02	-0.10	-0.07	**0.20**$^{\#}$	0.18	0.04
PDO	0.18	0.16	0.07	-0.01	**-0.20**$^{\#}$	-0.05	-0.01	-0.14	0.20	0.01	0.07	0.09
POL	-0.17	**-0.26***	**-0.20**$^{\#}$	**-0.34****	-0.16	0.13	0.06	0.05	**0.20**$^{\#}$	-0.08	0.08	0.04
SCA	-0.15	**-0.42****	**-0.46****	-0.12	**-0.56****	**-0.49****	-0.10	**-0.33****	**-0.39****	**-0.21**$^{\#}$	**0.21**$^{\#}$	**-0.39****

Table 4. The years corresponding to the low values of the seasonal SPEI3 PCs (< -1 std. dev.) and high values (> 1 std. dev.) used for the composite map analysis in Section 4.

DJF						**MAM**						**JJA**						**SON**					
PC1		**PC2**		**PC3**		**PC1**		**PC2**		**PC3**		**PC1**		**PC2**		**PC3**		**PC1**		**PC2**		**PC3**	
Low	High	Low	High	Low	High	Low	High	Low	High	Low	High	Low	High	Low	High	Low	High	Low	High	Low	High	Low	High
1903	1916	1904	1914	1912	1905	1911	1922	1915	1903	1903	1915	1911	1907	1902	1920	1904	1910	1904	1905	1906	1907	1909	1906
1909	1924	1908	1918	1915	1914	1918	1937	1916	1921	1904	1929	1914	1916	1909	1921	1911	1912	1907	1923	1910	1917	1924	1908
1921	1936	1919	1949	1930	1922	1921	1958	1919	1934	1905	1932	1915	1927	1913	1931	1921	1914	1920	1925	1912	1921	1938	1921
1925	1948	1920	1952	1935	1923	1923	1962	1923	1938	1910	1933	1917	1928	1916	1936	1923	1926	1921	1927	1913	1923	1939	1928
1932	1953	1926	1973	1936	1934	1928	1966	1936	1943	1913	1938	1930	1931	1919	1938	1928	1927	1939	1930	1914	1929	1944	1933
1933	1955	1938	1974	1939	1940	1929	1970	1937	1945	1916	1941	1936	1935	1925	1939	1934	1930	1947	1935	1915	1932	1951	1945
1934	1961	1940	1975	1945	1942	1942	1977	1940	1949	1918	1944	1937	1945	1933	1946	1947	1933	1949	1940	1922	1935	1960	1947
1942	1966	1941	1976	1950	1948	1943	1983	1941	1953	1920	1953	1940	1958	1941	1954	1949	1936	1951	1950	1925	1942	1965	1948
1943	1967	1942	1983	1951	1953	1946	1992	1951	1961	1927	1955	1941	1961	1942	1957	1952	1941	1955	1952	1931	1948	1967	1953
1946	1968	1947	1984	1960	1963	1954	1994	1956	1989	1928	1956	1955	1962	1945	1961	1959	1958	1959	1954	1933	1953	1968	1959
1947	1975	1953	1989	1961	1968	1956	1995	1958	1990	1934	1958	1959	1981	1969	1963	1962	1965	1972	1957	1936	1954	1974	1969
1949	1981	1960	1990	1977	1976	1960	1998	1963	1992	1937	1963	1963	1985	1978	1972	1976	1966	1975	1960	1939	1961	1975	1971
1954	1982	1963	1992	1983	1981	1963	2000	1969	1993	1947	1964	1969	1987	1980	1979	1989	1972	1976	1974	1941	1962	1987	1973
1964	2010	1969	1993	1994	1989	1969	2001	1970	1997	1950	1973	1971	1998	1985	1981	1994	1980	2005	1980	1960	1967	1994	1977
1972	2011	1970	1997	2001	1992	1972	2008	1978	2000	1972	1976	1975	2000	1997	1992	1996	1985		1981	1968	1982	2000	1978
1973		1977	2000		2002	1974		1979	2003	1986	1980	1976	2007		1999	2003	1997		1984	1972	1983	2001	1985
1996		1996	2002		2011	1976		1980	2011	1988	1993	1992	2009		2002		1999		1998	1976	1985	2005	1989
		2003	2007			1984			2012	1989	1997	2006	2012		2007		2002			1996	1986		1990
		2010	2008			1996				2002	2004				2010					2002	2011		1997
			2012			2003					2005										2012		2003
						2011					2010												
											2012												
17	**15**	**19**	**20**	**15**	**17**	**21**	**15**	**17**	**18**	**19**	**22**	**18**	**18**	**15**	**19**	**16**	**18**	**14**	**17**	**19**	**20**	**17**	**20**